Quantum wavelength-division-multiplexing and multiple-access communication systems and networks: Global and unified approach

Marzieh Bathaee,[1,*] Mohammad Rezai,[1,2,†] and Jawad A. Salehi[1,2,3,‡]
[1]*Sharif Quantum Center, Sharif University of Technology, Tehran 14588-89694, Iran*
[2]*Institute for Convergence Science & Technology, Sharif University of Technology, Tehran 14588-89694, Iran*
[3]*Electrical Engineering Department, Sharif University of Technology, Tehran 11155-4363, Iran*

(Received 14 June 2022; accepted 6 January 2023; published 20 January 2023)

The march towards successful global quantum internet requires introducing all-quantum networks and signal processing techniques. In this paper, we develop and discuss methods for various wavelength-division-multiplexing and multiple-access (WDM) communication systems and networks in fully quantum mechanical terms to obtain all-quantum WDM (QWDM) systems and networks. We begin the paper with a detailed discussion on various possible narrow-band and wideband sources of light signals used in typical WDM systems, such as coherent, number, and Poissonian mixed states. After introducing a generic and fully quantum mechanical WDM network, we develop methodologies for obtaining the necessary mathematical evolutions through wavelength distributors such as arrayed-waveguide-grating multiplexers and demultiplexers, and wavelength-sensitive and -insensitive broadcasting star couplers. In particular, using the methodologies introduced, one can use the results to obtain a complete and exact expression for any evolved pure quantum light signal through a typical WDM network using the aforementioned optical components. To test the validity and robustness of our mathematical expression for the evolved QWDM light signals, we use two opposing and extreme signals, namely, coherent state and number state, as inputs to various WDM communication and network systems and architecture. The methodologies and the required mathematical QWDM models introduced here can be extended to any fully quantum network architecture deemed necessary in a future global quantum internet, e.g., fiber to the home, Lambdanet-based broadcast WDM networks, and quantum routers based on a waveguide grating router.

DOI: 10.1103/PhysRevA.107.012613

I. INTRODUCTION

The successful emergence of various quantum communication systems and networks in the futuristic quantum internet will highly depend on developing all-quantum signal processing techniques and models embedded in quantum network applications [1–3]. All-quantum signal processing techniques within vast and complex networks face many challenges due to the wide range of optical and photonic devices and subsystems used in such networks. The core challenge in developing all-quantum signal processing in the aforementioned networks lies in preserving the quantumness of the state of quantum light to keep its quantum advantage while transforming from one module (device) to another with different functionalities. For example, in a typical multiuser wavelength-division-multiplexing (WDM) network, due to multiple users, an array of output quantum light sources needs to pass through an arrayed waveguide grating (AWG) device followed by a broadcasting star coupler, and prior to detection, the array passes through optical routers and filters [4]. In an all-quantum network, one needs to describe the evolution of the quantum state of light at each stage of the network prior to entering the next stage, thereby making the development of such techniques with a precise mathematical model into a Herculean task.

Due to its immense bandwidth, optical fiber communication systems and networks dominate the essential backbone and the building blocks of today's global communication networks. The wide bandwidth in optical fiber makes it possible to send information on channels with different wavelengths in a single optical fiber. Using WDM techniques, classical bits of information associated with different users are independently modulated on a particular wavelength with a specific frequency space from the other user's channel. WDM is one of the principal methodologies in conventional and global optical fiber communication networks [5], ranging from a point-to-point long-haul communication topology illustrated in Fig. 1(a) to local area networks such as the passive photonic loop and Lambdanet networks [6] depicted, respectively, in Figs. 1(b) and 1(c) [7]. In the passive photonic loop [Fig. 1(b)], different wavelengths (channels) are distributed among the end users by multiplexing and demultiplexing of the wavelengths. On the other hand, in the Lambdanet network [Fig. 1(c)], a star coupler broadcasts the wavelengths among many end users. Extensive works have been done thus far related to adapting WDM techniques for quantum communication systems [8–11].

Like the conventional classical network, any quantum network requires a backbone in charge of connecting

*neda.bathaee@gmail.com
†m.rezai@ee.sharif.edu
‡jasalehi@sharif.edu

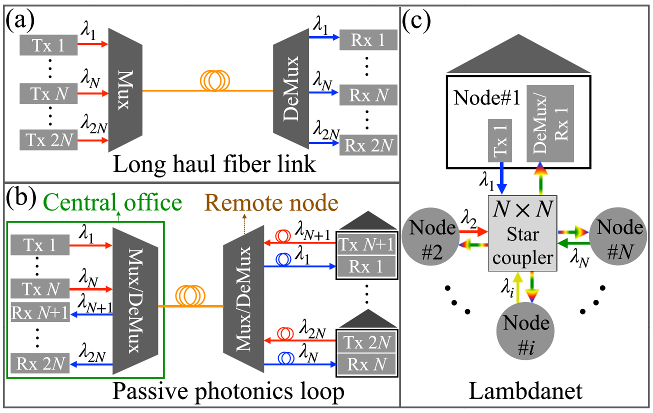

FIG. 1. (a) Wavelength division multiplexing optical network via a multichannel point-to-point long-haul fiber link [7], (b) passive photonic loop [7], and (c) single-hop WDM access network topologies (Lambdanet [6]). See Appendix A for more description. Tx and Rx, respectively, stand for transmitter and receiver systems. Mux and DeMux are abbreviations of multiplexing and demultiplexing, respectively.

long-distance nodes to local networks, including access networks such as fiber-to-the-home (FTTH) networks [12,13]. The access networks connect every two local users via various topologies. In point-to-multipoint network topologies, users exchange information indirectly through a central node at a higher rate, while in the multipoint-to-multipoint scheme, all users connect directly or via a star coupler or arrayed waveguide gratings. In addition, different dimensions such as time, frequency, wavelength, code, and space can be employed for assigning a unique channel to different users [14–18]. The two key properties of access network topologies are cost effectiveness and reliability. In this regard, passive optical networks (PONs), which utilize passive network elements such as optical power splitters and combiners and wavelength multiplexers and demultiplexers, have also been adapted for quantum local networks and quantum key distribution (QKD) networks [19–25]. As a result of the possibility of utilizing existing optical fiber infrastructure economically, quantum engineers are increasingly investigating quantum and classical network hybridization [26–29]. Therefore, investigating the same existing classical networks for usage in quantum communications could be intriguing and quite challenging, since the consolidation between conventional and quantum channels without proper modifications could considerably degrade the quantum channel performance. As a result of the hybridization of strong classical and weak quantum signals, communication systems encounter serious challenges related to crosstalk and noise. However, there are various methods, engineering approaches, and protocols to overcome these difficulties; for example, by choosing proper channel spacing, we can dissociate classical WDM networks from quantum WDM networks [29]. Therefore, this paper focuses on the networks containing only quantum signals and their evolution in the QWDM networks.

In this paper, we study all-quantum multiaccess WDM (QWDM) communication systems. In the context of QWDM, we develop a systematic approach to the evolution of generic quantum signals among WDM devices. The quantum operation of a general WDM quantum communication system, which includes quantum transmitters, a passive quantum wavelength distributor, and quantum receivers, is analyzed. Hence, the operation of various possible configurations of passive quantum wavelength distributors in fully quantum terms is realizable. We further assume that the quantum transmitters prepare individual quantum light signals, and at the quantum receiver end, each quantum receiver measures its corresponding transmitted signal; this scheme is known as a *prepare-and-measure* quantum communication system [30]. Indeed, the upcoming futuristic internet requires entanglement-based networks utilizing quantum repeaters specifically in long-haul communications [31–33]. For the entanglement-based networks, one requires revisiting the methodologies and modeling introduced in this paper. However, this work focuses on prepare-and-measure access networks.

The paper is organized as follows. Section II analyzes the evolution of quantum signals in a generic QWDM communication system. Section III qualitatively discusses the evolution of wave-packet creation operators through QWDM networks. We examine three particular input states, coherent, mixed Poissonian, and single-photon states, in Sec. IV. We study the measurement results for coherent, single-photon, and mixed Poissonian states based on spectral intensity and projective measurements, respectively, in Sec. V. Finally, we conclude the paper in Sec. VI.

We would like to emphasize that our methodologies can be applied to various applications based on QWDM, such as QWDM Lambdanet broadcasting, router-based scheme (WGR), and the quantum counterpart of conventional FTTH topologies.

II. GENERAL QWDM NETWORK

As depicted in Fig. 2, the building block of a passive quantum communication system based on WDM consists of N quantum transmitters (QTx) emitting quantum signals toward a global $N \times N$ quantum wavelength distributor component ($\underline{\mathrm{G}}$). Then, the evolved quantum light-wave signals at the output of $\underline{\mathrm{G}}$ are guided to N local quantum receivers (QRx), where their outputs are detected by each receiver's quantum detector (QD). We assume unitary operators $\underline{\mathrm{G}}$ and $\underline{\mathrm{QR}}_j$ as lossless devices. However, the lossy devices can also be mathematically modeled by unitary operators with the help of adding extra ancillary ports as external degrees of freedom coming from the interaction of the ambient environment surrounding the devices [34–36]. Moreover, one can model the transmittance loss of the network inside the receiver losses [35,37].

Theorem 1. Consider a prepare-and-measure-based QWDM network depicted in Fig. 2. Let each transmitter i prepare a pure quantum state of light signal with an arbitrary normalized wave packet $\zeta_i(\omega)$ and a function of creation modes $\hat{a}^{\dagger(1)}_{i,\zeta_i}$ as $|\psi_{\zeta_i}\rangle^{(1)} = f_i(\hat{a}^{\dagger(1)}_{i,\zeta_i})|0\rangle$, where f_i is an arbitrary analytical function that leads to normalized quantum states. Then the simultaneous evolution of all transmitters' signals

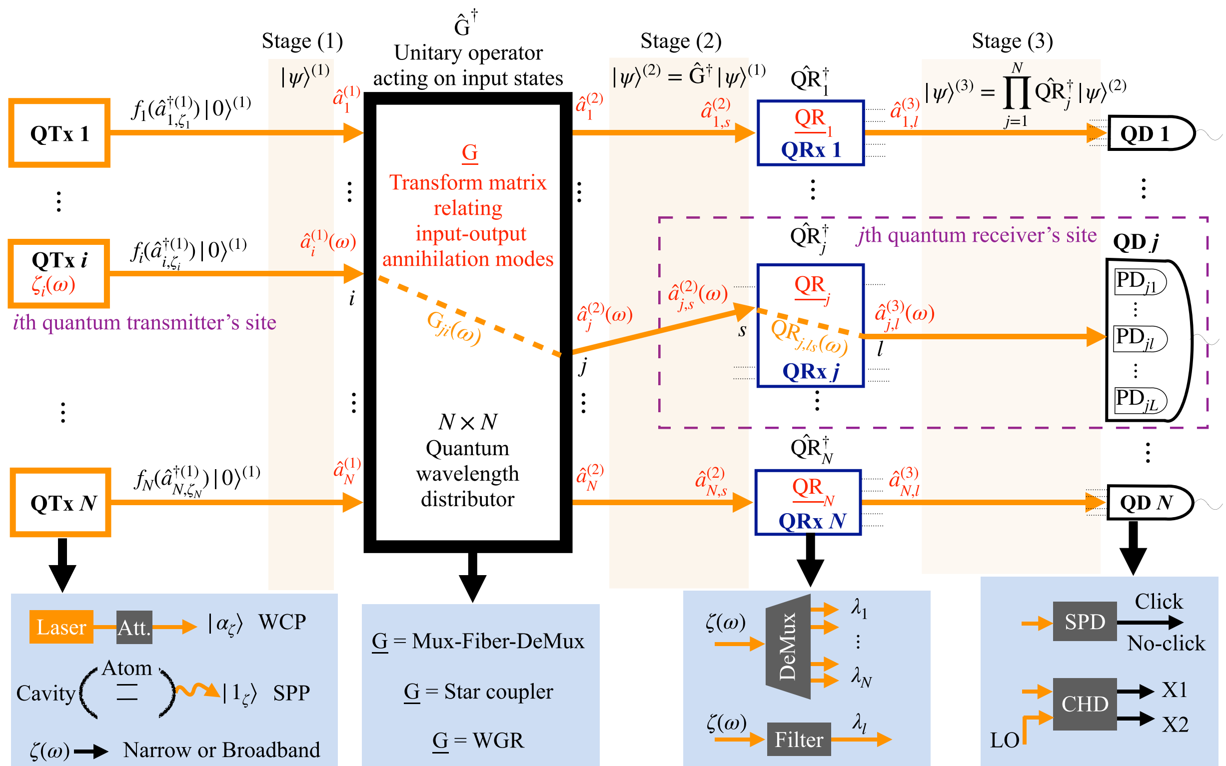

FIG. 2. Schematic of a generic quantum wavelength division multiplexing (QWDM) network. Depending on chosen network topology, G can be a star coupler, a combination of multiplexer/fiber/demultiplexer, and or a wavelength grating router (WGR). Depending on opted G, quantum transmitters (QTs) can be narrow and/or broadband lasers or single-photon sources. Input signals can be either weak coherent pulses (WCHs) or single-photon pulses (SPPs). Quantum receivers (QR), depending on a particular choice of G, are a demultiplexer and/or a single frequency filter. Quantum detectors (QDs) can be either single-photon detectors (SPDs) or conjugate homodyne detectors (CHDs). PD_{jl} stands for a photodetector that receives the optical signal from the lth output of the jth receiver. LO is a local oscillator. X1 and X2 indicate field quadratures.

through the global quantum wavelength distributer $\hat{\mathrm{G}}^{\dagger}$ and local quantum receivers $\hat{\mathrm{QR}}^{\dagger}$ results in receivers' signals as

$$|\psi\rangle^{(3)} = \prod_{i=1}^{N} f_i\left(\sum_{j=1}^{N} \mathrm{G}_{ji}(\zeta_i)\sum_{l=1}^{L}\mathrm{QR}_{j,ls}(\eta_{ji})\hat{a}^{\dagger(3)}_{j,l,\gamma_{lsji}}\right)|0\rangle,$$

where η_{ji} and γ_{lsji} are the normalized wave packets of signals after evolution from the global operator $\hat{\mathrm{G}}^{\dagger}$ and the local operators $\hat{\mathrm{QR}}^{\dagger}$, respectively. The superscripts (1), (2), and (3) indicate the signal evolution in three stages, namely, (1) after quantum transmitters, (2) after the quantum wavelength distributor, and (3) after quantum receivers.

Proof. The simultaneous evolution of input signals in a generic QWDM network, as depicted in Fig. 2, is obtained through three stages in Secs. II A–II C.

A. QWDM signal sources

Any generic communication network consists of signals carrying information transmitted by senders to their corresponding receivers. It is, therefore, essential to accurately describe the signals that carry information. In QWDM networks, quantum signals are distinguished by their frequency contents and quantum states. The former indicates the quantum signal's spectrum, and the latter specifies the photon number distribution of the quantum signal.

A typical pure state of a monochromatic single-mode lightwave signal is written as $|\psi\rangle = \sum_{n=0}^{\infty} c_n|n\rangle$, where $|n\rangle$ is the number state that can be written according to the monochromatic single-mode creation operator $\hat{a}^{\dagger}$ acting n times on the vacuum state $|0\rangle$ as $|n\rangle = \frac{\hat{a}^{\dagger n}}{\sqrt{n!}}|0\rangle$. However, since there is no perfect monochromatic single-mode source, signals are described with the help of wave-packet representations, which contain a finite bandwidth spectrum of a field mode. Thereby, the annihilation and creation operators related to the normalized finite bandwidth spectrum $\zeta(\omega)$ are written as [38]

$$\hat{a}_{\zeta} = \int_{-\infty}^{\infty} \zeta^*(\omega)\hat{a}(\omega)\,d\omega, \tag{1a}$$

$$\hat{a}_{\zeta}^{\dagger} = \int_{-\infty}^{\infty} \zeta(\omega)\hat{a}^{\dagger}(\omega)\,d\omega, \tag{1b}$$

where $\hat{a}(\omega)$ and $\hat{a}^{\dagger}(\omega)$ are the annihilation and creation operators, corresponding to the frequency ω, and the commutation relation $[\hat{a}_{\zeta}, \hat{a}_{\zeta}^{\dagger}] = 1$ is fulfilled due to the normalized spectral wave-packet $\zeta(\omega)$ condition $\int_{-\infty}^{\infty} |\zeta(\omega)|^2\,d\omega = 1$. Besides, other degrees of freedom related to field modes, such as polarization and orbital angular momentum (structured light), can be considered as additional indices on $\hat{a}_\zeta$ [39–41]. As a result, any signal prepared in an arbitrary pure state is given by

$$|\psi_\zeta\rangle = \sum_{n=0}^{\infty} c_n|n_\zeta\rangle = \sum_{n=0}^{\infty} \frac{c_n}{\sqrt{n!}}\hat{a}_\zeta^{\dagger n}|0\rangle = f(\hat{a}_\zeta^\dagger)|0\rangle, \quad (2)$$

where f is an analytical function specified by coefficients c_n [18,42]. For instance, consider two prevalent pure states in quantum optics and engineering: coherent states,

$$|\alpha_\zeta\rangle = e^{-|\alpha|^2/2}\sum_{n=0}^{\infty}\frac{\alpha^n}{n!}\hat{a}_\zeta^{\dagger n}|0\rangle, \quad (3)$$

and single-photon states,

$$|1_\zeta\rangle = \hat{a}_\zeta^\dagger|0\rangle. \quad (4)$$

Accordingly, the coefficients c_n of f associated with the coherent and single-photon states can be easily determined. It is worth noting that the coherent state can also be represented by acting unitary displacement operator

$$\hat{D}(\alpha\zeta) = \exp[\alpha\hat{a}_\zeta^\dagger - \alpha^*\hat{a}_\zeta] \quad (5)$$

on the vacuum state, which is related to the function f as

$$|\alpha_\zeta\rangle = f(\hat{a}_\zeta^\dagger)|0\rangle = \exp\left[-\frac{|\alpha|^2}{2} + \alpha\hat{a}_\zeta^\dagger\right]|0\rangle = \hat{D}(\alpha\zeta)|0\rangle, \quad (6)$$

by use of Baker-Campbell-Hausdorff formula in addition to the relations $[\hat{a}(\omega), \hat{a}^\dagger(\omega')] = \delta(\omega-\omega')$, and $\hat{a}(\omega)|0\rangle = 0$. Since the displacement operator, $\hat{D}(\alpha)$, is a unitary operator that simplifies mathematical manipulations, in this paper, whenever the signals are in coherent states, f is replaced with the displacement operator according to Eq. (6).

Quantum sources can also be classified as narrow- and broad-bandwidth sources. For the former, it is assumed the central frequency of the wave packet ω_c is sufficiently larger than the bandwidth $\Delta\omega$, i.e., $\omega_c \gg \Delta\omega$. On the other hand, broad-bandwidth sources involve several different frequency (wavelength) components.

The output signals of lasers, as conventional sources in optical and quantum communications, are approximated by a coherent state with a spectral density described by a Voigt function (convolution between a Gaussian and a Lorentzian function) [43]. For example, near the center of the spectrum corresponding to a diode laser, the absolute square of the wave packet of the output signal is approximated by Gaussian profile $|\zeta(\omega)|^2 = \sqrt{\frac{1}{\pi\Delta\omega^2}}e^{-(\omega-\omega_c)^2/\Delta\omega^2}$. In contrast, the Lorentzian profile $|\zeta(\omega)|^2 = \frac{1}{\pi}\frac{\Delta\omega}{(\omega-\omega_c)^2+\Delta\omega^2}$ describes the output signal spectrum near the tails of the line shape. As highlighted, a single-photon source is the other practical quantum source that has many applications in quantum information processing as well as secure quantum communications. Several configurations and experimental demonstrations have been performed to fabricate an ideal quantum single-photon source [44]. One of these can be an atom-cavity system where the cavity transmission profile can adjust the spectrum width of the single-photon source [45]. Furthermore, a broadband entangled photon source generated by a spontaneous parametric down-conversion procedure can also introduce a heralded broad-bandwidth single photon [46].

Despite the availability of single-photon sources, they still have to overcome some technological challenges to become commercially available communication sources. Alternatively, weak coherent states with random phases generated via a commercial laser followed by a phase randomizer and an attenuator can emulate a single-photon state for some specific applications [47]. Nevertheless, this state is no longer a pure state, and indeed it is a mixed state with Poissonian distribution as follows [48]:

$$\rho_C = \frac{1}{2\pi}\int_o^{2\pi}|\alpha_\zeta\rangle\langle\alpha_\zeta|\,d\phi = e^{-|\alpha|^2}\sum_{n=0}^{\infty}\frac{|\alpha|^{2n}}{n!}|n_\zeta\rangle\langle n_\zeta|. \quad (7)$$

For weak coherent pulses, it is assumed the mean photon number $|\alpha|^2 \ll 1$, where $\alpha = |\alpha|e^{i\phi}$. The Poissonian mixed states are signals used in decoy state-QKD protocols [49].

B. QWDM signal evolution through a global wavelength distributor

According to Fig. 2, in a generic QWDM network, quantum signals are independently prepared by each quantum transmitter and are received by individual receivers. Meanwhile, the global state prepared by all transmitters experiences three stages prior to reaching their corresponding receivers' detectors. The global state in stage 1 is the tensor product of all prepared states by each transmitter as

$$|\psi\rangle^{(1)} = \prod_{i=1}^{N}|\psi_{\zeta_i}\rangle^{(1)} = \prod_{i=1}^{N} f_i(\hat{a}_{i,\zeta_i}^{\dagger(1)})|0\rangle^{(1)}, \quad (8)$$

where the subscript i indicates that the ith quantum transmitter emits a quantum signal with photon number distribution specified by f_i, and its wave-packet profile ζ_i. Besides, the vacuum state in stage 1 is denoted by $|0\rangle^{(1)} = |0,\dots,0\rangle^{(1)}$, where the total number of zeros is equal to N [18]. Then, $|\psi\rangle^{(1)}$ passes through the global unitary operator $\hat{G}^\dagger$ corresponding to a wavelength distributor. As a result, the correlated output state in stage 2 becomes

$$\begin{aligned}|\psi\rangle^{(2)} = \hat{G}^\dagger|\psi\rangle^{(1)} &= \prod_{i=1}^{N}\hat{G}^\dagger f_i(\hat{a}_{i,\zeta_i}^{\dagger(1)})\hat{G}|0\rangle^{(1)}\\ &= \prod_{i=1}^{N} f_i(\hat{G}^\dagger\hat{a}_{i,\zeta_i}^{\dagger(1)}\hat{G})|0\rangle^{(1)}, \end{aligned}\quad (9)$$

where the unitary operator $\hat{G}^\dagger$ leads to the evolution of the state in the Schrödinger picture, i.e., $|\psi\rangle^{(1)} \xrightarrow{\hat{G}^\dagger} |\psi\rangle^{(2)}$. It is important to note that, in Eq. (9), the term $\hat{G}^\dagger\hat{a}_{i,\zeta_i}^{\dagger(1)}\hat{G}$ can be realized as the quantum evolution of the creation operator $\hat{a}_{i,\zeta_i}^{\dagger(1)}$ with respect to the unitary evolution operator $\hat{G}$ (not $\hat{G}^\dagger$) in the Heisenberg picture, i.e., $\hat{a}_{i,\zeta_i}^{\dagger(1)} \xrightarrow{\hat{G}} \hat{G}^\dagger\hat{a}_{i,\zeta_i}^{\dagger(1)}\hat{G}$. The representation of the term $\hat{G}^\dagger\hat{a}_{i,\zeta_i}^{\dagger(1)}\hat{G}$ based on the output creation modes of the system is

$$\hat{G}^\dagger \hat{a}_i^{\dagger(1)}(\omega)\hat{G} = \sum_{j=1}^{N} G_{ji}(\omega)\, \hat{a}_j^{\dagger(2)}(\omega), \tag{10}$$

where $G_{ji}(\omega)$ are the elements of the transform matrix $\underline{G}(\omega)$. The mathematical details leading to Eq. (10) are reviewed in Appendix B and follow the same approach as given in Ref. [18]. Now, by use of Eqs. (1b) and (10), the term $\hat{G}^\dagger \hat{a}_{i,\zeta_i}^{\dagger(1)}\hat{G}$ is written based on the output creation modes as

$$\begin{aligned}\hat{G}^\dagger \hat{a}_{i,\zeta_i}^{\dagger(1)}\hat{G} &= \int \zeta_i(\omega) \sum_{j=1}^{N} \hat{G}^\dagger \hat{a}_i^{\dagger(1)}(\omega)\hat{G}\, d\omega \\ &= \sum_{j=1}^{N} \int \zeta_i(\omega) G_{ji}(\omega)\hat{a}_j^{\dagger(2)}(\omega)\, d\omega \\ &= \sum_{j=1}^{N} G_{ji}(\zeta_i)\hat{a}_{j,\eta_{ji}}^{\dagger(2)}. \end{aligned}\tag{11}$$

In Eq. (11), the creation mode $\hat{a}_{j,\eta_{ji}}^{\dagger(2)}$ related to the modified normalized wave packet $\eta_{ji}(\omega)$ is defined as

$$\hat{a}_{j,\eta_{ji}}^{\dagger(2)} = \int \eta_{ji}(\omega)\hat{a}_j^{\dagger(2)}(\omega)\, d\omega, \tag{12}$$

where

$$\eta_{ji}(\omega) = \zeta_i(\omega) G_{ji}(\omega)/G_{ji}(\zeta_i), \tag{13a}$$

$$G_{ji}(\zeta_i) = e^{i\phi_{ji}} \sqrt{\int |\zeta_i(\omega')|^2 |G_{ji}(\omega')|^2\, d\omega'}. \tag{13b}$$

The phase ϕ_{ji} is a specific parameter that guarantees the unitarity of the matrix made by elements $G_{ji}(\zeta_i)$. The interrelationship between the coefficients $G_{ji}(\zeta_i)$ and $G_{ji}(\omega)$ is discussed in Appendix C.

As a result, by inserting Eq. (11) into Eq. (9), the state in stage 2 becomes

$$|\psi\rangle^{(2)} = \prod_{i=1}^{N} f_i \left(\sum_{j=1}^{N} G_{ji}(\zeta_i)\hat{a}_{j,\eta_{ji}}^{\dagger(2)} \right) |0\rangle^{(2)}. \tag{14}$$

The superscript (2) on the creation operators written in Eqs. (11) and (14) indicates the system has evolved to stage 2.

C. Outputs of quantum wavelength demultiplexers and filters

This section considers the evolution of signals towards stage 3. In this regard, the multiplication of all local unitary operators, i.e., $\hat{QR}^\dagger = \prod_{j=1}^{N} \hat{QR}_j^\dagger$, where $\hat{QR}_j^\dagger$ corresponds to the jth quantum wavelength demultiplexers and filters, acts on the global state $|\psi\rangle^{(2)}$ as

$$|\psi\rangle^{(3)} = \hat{QR}^\dagger |\psi\rangle^{(2)} = \prod_{j=1}^{N} \hat{QR}_j^\dagger |\psi\rangle^{(2)}. \tag{15}$$

To determine $|\psi\rangle^{(3)}$, the linear transform matrix $\underline{QR}_j$ corresponding to $\hat{QR}_j^\dagger$ is characterized by an $L \times L$ unitary matrix, where $L \geqslant \min\{k+1, K\}$ and $1 \leqslant k \leqslant K$ is the number of wavelengths that the jth user's receiver chooses to have, and the maximum number of the wavelengths that the communication system can support is K, where $K \leqslant N$. For example, for a single wavelength narrow-band filter, $k = 1$ and the $\underline{QR}_j$ can be mathematically modeled by a 2×2 unitary transform matrix where the first input of the filter passes the filter frequency towards the first output and the second output emits all other frequency components of the input signal. Incidentally, an ideal $K \times K$ quantum demultiplexer can also be a good model for a filter where we assume one of its output ports related to the filter frequency is open (detected), and the remaining outputs are blocked. Without loss of generality, in this paper, every quantum receiver $\underline{QR}_j$ is modeled by an identical $L \times L$ demultiplexer where $L = K$ (see Appendix D).

Here the same mathematical steps are performed as in Appendix B [Eqs. (B1)–(B6)], only $\hat{QR}^\dagger$ is replaced by $\hat{G}^\dagger$, and the mode evolution between stages 2 and 3 is accounted for. Moreover, since the output of $\underline{G}$ is connected to one of the inputs of $\underline{QR}_j$ labeled by s, this label as an additional subindex must be considered to the related creation modes as $\hat{a}_{j,\eta_{ji}}^{\dagger(2)} \to \hat{a}_{j,s,\eta_{ji}}^{\dagger(2)}$ and it is important to note that $\hat{a}_{j,\eta_{ji}}^{\dagger(2)} \equiv \hat{a}_{j,s,\eta_{ji}}^{\dagger(2)}$ (without considering the transmittance loss). In other words, we are dealing with the same field operator coming out of the port j of $\underline{G}$ to the input port s of $\underline{QR}_j$. We also assume label s is the same for all quantum receivers $\underline{QR}_j$s. To realize why this assumption does not impose any restriction on our model, see Appendix D.

From the above discussion, one can write the relation between input creation mode $\hat{a}_{j,s}^{\dagger(2)}(\omega)$ related to port s and output creation modes $\hat{a}_{j,l}^{\dagger(2)}(\omega)$ due to the quantum receiver operator $\hat{QR}_j^\dagger$ as

$$\hat{QR}_j^\dagger \hat{a}_{j,s}^{\dagger(2)}(\omega)\hat{QR}_j = \sum_{l=1}^{L} QR_{j,ls}(\omega)\, \hat{a}_{j,l}^{\dagger(3)}(\omega), \tag{16}$$

and the output wave packet of $\underline{G}$ given in Eq. (12) is rewritten as

$$\hat{a}_{j,s,\eta_{ji}}^{\dagger(2)} = \int \eta_{ji}(\omega)\hat{a}_{j,s}^{\dagger(2)}(\omega)\, d\omega. \tag{17}$$

Therefore, according to Eqs. (16) and (17) the unitary operator $\hat{QR}_j^\dagger$ gives rise to the evolution of the wave-packet creation mode $\hat{a}_{j,s,\eta_{ji}}^{\dagger(2)}$, in the following form:

$$\begin{aligned}\hat{QR}_j^\dagger \hat{a}_{j,s,\eta_{ji}}^{\dagger(2)} \hat{QR}_j &= \int \eta_{ji}(\omega) \sum_{l=1}^{L} (\underline{QR}_j^\dagger(\omega))^*_{sl} \hat{a}_{j,l}^{\dagger(3)}(\omega)\, d\omega \\ &= \sum_{l=1}^{L} \int \eta_{ji}(\omega) QR_{j,ls}(\omega)\hat{a}_{j,l}^{\dagger(3)}(\omega)\, d\omega \\ &= \sum_{l=1}^{L} QR_{j,ls}(\eta_{ji})\hat{a}_{j,l,\gamma_{lsji}}^{\dagger(3)}, \end{aligned}\tag{18}$$

where in Eq. (18), another normalized modified wave packet $\gamma_{lsji}(\omega)$ related to the photon-wave-packet creation mode

$$\hat{a}_{j,l,\gamma_{lsji}}^{\dagger(3)} = \int \gamma_{lsji}(\omega)\hat{a}_{j,l}^{\dagger(3)}(\omega)\, d\omega \tag{19}$$

is defined as

$$\gamma_{lsji}(\omega) = \eta_{ji}(\omega)\mathrm{QR}_{j,ls}(\omega)/\mathrm{QR}_{j,ls}(\eta_{ji}), \tag{20a}$$

$$\mathrm{QR}_{j,ls}(\eta_{ji}) = e^{i\phi'_{ls}}\sqrt{\int |\eta_{ji}(\omega')|^2|\mathrm{QR}_{j,ls}(\omega')|^2\, d\omega'}. \tag{20b}$$

In Eq. (20b), the phase ϕ'_{ls} is accounted for to obtain the unitarity matrix $\underline{\mathrm{QR}}_j(\eta_{ji})$ (see Appendix C). Note that $\hat{a}^{\dagger(3)}_{j,l}(\omega)$ is the creation operator of frequency ω related to the jth receiver at the output port number l of the $\hat{\mathrm{QR}}_j$. The subscript s is a fixed input port number for all $\underline{\mathrm{QR}}_j$s ($\hat{a}^{\dagger(2)}_{j,\eta_{ij}} \equiv \hat{a}^{\dagger(2)}_{j,s,\eta_{ij}}\ \forall j$). Consequently, the state before each quantum detector (QD) is a correlated state which is not separable in general. Accordingly, the global state at stage 3, the output of the quantum network, becomes

$$\begin{aligned}
|\psi\rangle^{(3)} &= \hat{\mathrm{QR}}^\dagger|\psi\rangle^{(2)} = \hat{\mathrm{QR}}^\dagger\hat{\mathrm{G}}^\dagger|\psi\rangle^{(1)}\\
&= \prod_{i=1}^{N} f_i(\hat{\mathrm{QR}}^\dagger\hat{\mathrm{G}}^\dagger\hat{a}^{\dagger(1)}_{i,\zeta_i}\hat{\mathrm{G}}\hat{\mathrm{QR}})|0\rangle^{(3)}\\
&= \prod_{i=1}^{N} f_i\left(\sum_{j=1}^{N}\mathrm{G}_{ji}(\zeta_i)\hat{\mathrm{QR}}_j^\dagger\hat{a}^{\dagger(2)}_{j,s,\eta_{ji}}\hat{\mathrm{QR}}_j\right)|0\rangle^{(3)}\\
&= \prod_{i=1}^{N} f_i\left(\sum_{j=1}^{N}\mathrm{G}_{ji}(\zeta_i)\sum_{l=1}^{L}\mathrm{QR}_{j,ls}(\eta_{ji})\hat{a}^{\dagger(3)}_{j,l,\gamma_{lsji}}\right)|0\rangle^{(3)}.
\end{aligned} \tag{21}$$

Equation (21) is an essential result of this paper. It presents a complete picture of the evolution of the transmitted quantum state of light through a generic QWDM network. The choices of $\hat{\mathrm{G}}^\dagger$ and $\hat{\mathrm{QR}}_j^\dagger$ indicate whether we want to use a passive optical star coupler [18] or arrayed waveguide grating multiplexers and demultiplexers or wavelength-sensitive filters [34] in our QWDM network. Various choices of $\hat{\mathrm{G}}^\dagger$ and $\hat{\mathrm{QR}}_j^\dagger$ will depend on the application and topology of our QWDM network.

Note that Eq. (21) (Theorem 1) is a general result that includes possible crosstalk effects among the frequency content of users' signals; for instance, these effects may arise from the wavelength distributor $\hat{\mathrm{G}}^\dagger$.

The main result of the evolution of quantum signals within the QWDM network is highlighted in the following.

Highlighting the main results. A prepare-and-measure QWDM network described in this work yields the following results:

(i) Assume various single-mode pure quantum signals given in Eq. (8) emitted by individual transmitters evolve within a generic WDM network presented in Fig. 2. In this case, the global and correlated quantum output state can be expressed by Eq. (21) (Theorem 1). Comparing Eq. (8) with Eq. (21), one can conclude the mode evolution is as follows:

$$\hat{a}^{\dagger(1)}_{i,\zeta_i} \to \sum_{j=1}^{N}\mathrm{G}_{ji}(\zeta_i)\sum_{l=1}^{L}\mathrm{QR}_{j,ls}(\eta_{ji})\hat{a}^{\dagger(3)}_{j,l,\gamma_{lsji}}.$$

(ii) The imperfect devices can be mathematically modeled by adding extra input ports related to the ambient medium. Therefore, for any imperfect network device, it can also be described by unitary operators considered in this work by $\underline{\mathrm{G}}$ and $\underline{\mathrm{QR}}_j$. For the auxiliary ports used to model system-environment interaction, the corresponding inputs are substituted by the vacuum states, i.e., $f_i(\hat{a}^{\dagger(1)}_{i,\zeta_i})) = 1$. These extra ports are responsible for vacuum fluctuations as well as loss. For instance, the vacuum noises degrade the signal-to-noise ratio of received signals in homodyne detection [50]. One can analyze these effects through Eq. (21) (Theorem 1).

(iii) Equation (21) (Theorem 1) also includes the crosstalk effects expressed in terms of the explicit form of $\underline{\mathrm{G}}$ and $\underline{\mathrm{QR}}_j$.

(iv) The evolution of mixed states, such as Poissonian mixed states or thermal states, which can be expressed based on the coherent state densities, is straightforward using Eq. (27b) (Corollary 1) (see Sec. IV B). Therefore, thermal noises arising from the environment can be modeled by entering a thermal state into the input port corresponding to the ambient environment [37].

D. Coexistence of quantum-classical signals

As mentioned briefly in the Introduction, the existing infrastructure of conventional WDM networks (Fig. 1) has a similar structure as a generic QWDM network depicted in Fig. 2. Therefore, hybridizing quantum and classical signals in the existing infrastructure is desirable since it would be cost effective. However, conventional signals that pass through these networks are strong classical optical signals since the launch power of these light sources must be such that it satisfies the classical receivers' sensitivity. Due to the higher intensity of the classical signals, the consolidation between conventional and quantum channels can degrade the quantum channel performance via background crosstalk noises [4,51].

Several methods have been proposed to reduce the background crosstalk in hybrid quantum-classical WDM networks so far, such as filtering methods in frequency and time domains [52,53], controlling the launch power of classical channels [52,53], inherent optical filtering (orthogonal frequency division multiplexing) [28], allocating higher wavelength to classical channels (O band) and lower wavelength to quantum channels (C band) [54], optimal wavelength assignment [29], and using dual feeder fibers [27].

For instance, Ref. [29] shows, by choosing a channel spacing of 200 GHz, the launch power of classical signals leading to the receiver's sensitivity −28 dBm or −25 dBm, and using proper narrow-band filters (15 and 125 GHz) on the quantum receivers, one can suppress the adverse effects of the background crosstalk noises.

As a result, classical and quantum signals can coexist in the conventional WDM infrastructure network using the above-mentioned methodologies. Therefore, without loss of generality, this paper only examines the quantum evolution of quantum signals in a generic QWDM network, assuming the utilization of the most optimum values of the classical launch power, channel spacing, and the narrow-band filter's bandwidth that can mitigate the quantum signal degradation by classical signals.

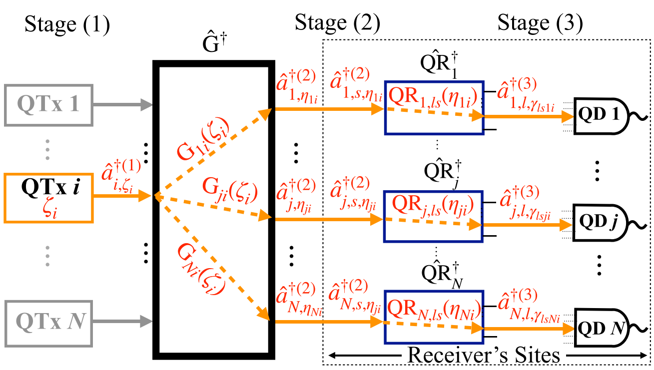

FIG. 3. Evolution of a single-photon wave-packet operator $\hat{a}^{\dagger(1)}_{i,\zeta_i}$ through a generic communication system's components towards all the receivers' detectors.

III. QUALITATIVE DISCUSSION ON WAVE-PACKET CREATION OPERATOR EVOLUTION

Figure 3 illustrates the evolution of a single-photon wave packet with spectral amplitude $\zeta_i(\omega)$ emitted by the ith transmitter through various stages of a QWDM system. As shown in Fig. 3, the quantum distributor $\hat{\mathrm{G}}^\dagger$ distributes a single photon with wave packet $\zeta_i(\omega)$ by weight of $\mathrm{G}_{ji}(\zeta_i)$ towards the jth receiver's site. Accordingly, the related wave packet is modified to $\eta_{ji}(\omega)$ in stage 2. Then, the new single-photon wave packet passes through the quantum receiver operator $\hat{\mathrm{QR}}^\dagger_j$. Therefore, in stage 3, we obtain the evolved single-photon wave packet denoted by $\gamma_{lsji}(\omega)$ in the lth output of the quantum receiver with the weight $\mathrm{QR}_{j,ls}(\eta_{ji})$. Therefore, the probability amplitude at stage 3 that the single-photon wave packet, specified by the normalized wave packet $\gamma_{lsji}(\omega)$, reaching the jth receiver, is determined by

$$\mathcal{N}_{lsji} = \mathrm{G}_{ji}(\zeta_i)\mathrm{QR}_{j,ls}(\eta_{ji}). \tag{22}$$

This definition simplifies Eq. (21) (Theorem 1) as follows:

$$|\psi\rangle^{(3)} = \prod_{i=1}^{N} f_i\left(\sum_{j=1,l=1}^{N,L} \mathcal{N}_{lsji}\hat{a}^{\dagger(3)}_{j,l,\gamma_{lsji}}\right)|0\rangle^{(3)}. \tag{23}$$

Each receiver operator discriminates its signals based on frequency content. For example, the spectral amplitude at output port jl [associated with creation operator $\hat{a}^{\dagger(3)}_{j,l}(\omega)$] from the ith transmitter equals the spectral amplitude of the ith transmitter's photon wave packet at output port jl, which is $\gamma_{lsji}(\omega)$, times the probability of the ith transmitter's photon arriving at the port jl, which is $\mathcal{N}_{lsji}$, i.e.,

$$\bar{\gamma}_{lsji}(\omega) = \mathcal{N}_{lsji}\gamma_{lsji}(\omega) = \mathrm{QR}_{j,ls}(\omega)\mathrm{G}_{ji}(\omega)\zeta_i(\omega), \tag{24}$$

where Eqs. (13a) and (20a) are used.

To sum up, $\mathcal{N}_{lsji}$ represents the total probability amplitude that a single photon with wave packet $\zeta_i(\omega)$ transmitted by the ith sender reaches the jth receiver along the s-l path of $\underline{\mathrm{QR}}_j$ (see Fig. 2). Correspondingly, $\bar{\gamma}_{lsji}(\omega)$ denotes the probability amplitude of each single photon with wave packet $\zeta_i(\omega)$ transmitted by the ith sender reaching the jth receiver at frequency ω.

IV. QWDM EXAMPLES BASED ON INPUT QUANTUM LIGHTS

Following are three corollaries resulting from Theorem 1 for three different inputs, coherent states, Poissonian mixed states, and single-photon states, prepared by all transmitters.

A. Coherent-state inputs

Corollary 1. According to Theorem 1, if all input signals are pure coherent states, the output signals become uncorrelated (tensor product) as

$$|\psi\rangle^{(3)}_{\mathrm{C}} = \prod_{j=1,l=1}^{N,L} \hat{D}\left(\sum_{i=1}^{N} \alpha_i\bar{\gamma}_{lsji}\right)|0\rangle^{(3)}.$$

Proof. As discussed before, for the coherent state, the displacement operator $\hat{D}$ replaces f_i [see Eq. (8)]. Using Eq. (24) and the relations

$$\left[\hat{a}^{(3)}_{j,l}(\omega), \hat{a}^{\dagger(3)}_{j',l'}(\omega')\right] = \delta_{jj'}\delta_{ll'}\delta(\omega-\omega'), \tag{25}$$

$$\hat{D}(\alpha_i\bar{\gamma}_{lsji} + \alpha_i\bar{\gamma}_{l'sj'i}) = \hat{D}(\alpha_i\bar{\gamma}_{lsji})\hat{D}(\alpha_i\bar{\gamma}_{l'sj'i}), \tag{26}$$

Eq. (21) (Theorem 1) becomes

$$\begin{aligned}
|\psi\rangle^{(3)}_{\mathrm{C}} &= \hat{\mathrm{QR}}^\dagger\hat{\mathrm{G}}^\dagger\prod_{i=1}^{N}\hat{D}(\alpha_i\zeta_i)|0\rangle^{(1)} \\
&= \prod_{i=1}^{N}\hat{D}\left(\sum_{j,l=1}^{N,L}\alpha_i\bar{\gamma}_{lsji}\right)|0\rangle^{(3)} \\
&= \prod_{i=1,j=1,l=1}^{N,N,L}\hat{D}(\alpha_i\bar{\gamma}_{lsji})|0\rangle^{(3)} \qquad (27a) \\
&= \prod_{j=1,l=1}^{N,L}\hat{D}\left(\sum_{i=1}^{N}\alpha_i\bar{\gamma}_{lsji}\right)|0\rangle^{(3)}. \qquad (27b)
\end{aligned}$$

Equation (27a) is a tensor product of $N\times N\times L$ coherent states distinguished by mode $\hat{a}^{\dagger(3)}_{j,l,\gamma_{lsji}}$. Equation (27b) is reduced to the tensor product of $N\times L$ displacement operators, $\hat{D}(\sum_{i=1}^{N}\alpha_i\bar{\gamma}_{lsji})$, corresponding to N distinct output ports of $\underline{\mathrm{G}}$ and L output ports of $\underline{\mathrm{QR}}_j$. Thus, Eq. (27b) (Corollary 1) shows no correlation between the states at the outputs of all quantum receivers ($\underline{\mathrm{QR}}_j$s) indicated by two indices j and l. In other words, the final state is separable, and there is no entanglement between different jl output ports of quantum receivers ($\underline{\mathrm{QR}}_j$s).

B. Poissonian mixed-state inputs

In contrast to the evolution of the coherent states as communication system inputs, one can recognize correlations between receivers when the transmitters prepare the mixed state given in Eq. (7).

Corollary 2. According to Theorem 1, if all input signals are Poissonian mixed states, the output signals become correlated as

$$\rho_{\mathrm{C}}^{(3)} = \prod_{i=1}^{N} \int_0^{2\pi} \frac{d\phi_i}{2\pi} \prod_{j=1,l=1}^{N,L} \hat{D}(\alpha_i \bar{\gamma}_{lsji})|0\rangle^{(3)}\, {}^{(3)}\langle 0|\hat{D}^{\dagger}(\alpha_i \bar{\gamma}_{lsji}).$$

Proof. By use of Eq. (27) (Corollary 1) in this case, the state in stage 3 turns into

$$\begin{aligned}\rho_{\mathrm{C}}^{(3)} &= \hat{\mathrm{QR}}^{\dagger}\hat{\mathrm{G}}^{\dagger}\prod_{i=1}^{N}\rho_{\mathrm{C},i}^{(1)}\hat{\mathrm{G}}\,\hat{\mathrm{QR}}\\ &= \prod_{i=1}^{N}\int_0^{2\pi}\frac{d\phi_i}{2\pi}\hat{\mathrm{QR}}^{\dagger}\hat{\mathrm{G}}^{\dagger}\hat{D}(\alpha_i\zeta_i)|0\rangle^{(1)}\,{}^{(1)}\langle 0|\hat{D}^{\dagger}(\alpha_i,\zeta_i)\hat{\mathrm{G}}\,\hat{\mathrm{QR}}\\ &= \prod_{i=1}^{N}\int_0^{2\pi}\frac{d\phi_i}{2\pi}\prod_{j=1,l=1}^{N,L}\hat{D}(\alpha_i\bar{\gamma}_{lsji})|0\rangle^{(3)}\,{}^{(3)}\langle 0|\hat{D}^{\dagger}(\alpha_i\bar{\gamma}_{lsji}),\end{aligned} \tag{28}$$

where $\alpha_i = |\alpha_i|e^{i\phi_i}$ and the integration on ϕ_i is in charge of correlations between receivers' states.

The importance of analyzing the Poissonian mixed-state inputs rests on two facts. First, in practice, the coherent-state inputs require a common local oscillator to overcome random phases. On the other hand, due to random phases, Poissonian mixed-state inputs do not require any local oscillator. Therefore, it simplifies the implementation of QWDM systems. Second, the weak Poissonian mixed state is utilized widely in QKD networks in place of a single-photon state as a cost-effective source [49,55].

C. Single-photon inputs

Corollary 3. According to Theorem 1, if all input signals are single-photon states, the output signals can be quantum correlated (entangled) as

$$|\psi\rangle_{\mathrm{S}}^{(3)} = \prod_{i=1}^{N}\left(\sum_{j=1}^{N}\sum_{l=1}^{L}\mathcal{N}_{lsji}\hat{a}_{j,l,\gamma_{lsji}}^{\dagger(3)}\right)|0\rangle^{(3)}. \tag{29}$$

Proof. To derive Eq. (29), it suffices to replace $f_i(\hat{a}_{i,\zeta_i}^{\dagger(1)})$ with $\hat{a}_{i,\zeta_i}^{\dagger(1)}$ in Eq. (8) and to use Eq. (22). As is clear from Eq. (29), due to superposition among different mode operators $\hat{a}_{j,l,\gamma_{lsji}}^{\dagger(3)}$, the output states can gain quantum correlations (entanglement). Therefore, the received state at the jth receiver is necessarily no longer a pure state. The following two examples are worth noting. First, a quantum Lambdanet broadcasting communication system with a star coupler as its wavelength distributor entangles the input single-photon states. Second, in contrast, an ideal router as a wavelength distributor of a router-based communication system guides uncorrelated input single-photon states to separate outputs without introducing any correlation (entanglement).

It is noteworthy that the evolution of other pure states, such as the single-mode squeezed states, can be derived using Eq. (21) (Theorem 1) and writing the squeezed state based on the number states [56,57]. However, the evolution of two-mode squeezing states that are employed in quantum networks such as a Gaussian quantum network [32] requires a further generalization of Eq. (8).

V. QUANTUM WDM SIGNAL MEASUREMENT

The encoded information on the input signals can be extracted via quantum WDM signal measurement in each output port of a quantum receiver in the QWDM Network. The measurement on the final state of input lights at stage 3 is categorized by two different measurement schemes:

(a) We use the intensity measurement operator for the separable coherent state [Eq. (27b)].

(b) We use projection operators for potentially quantum-correlated single-photon states [Eq. (29)] and Poissonian mixed states [Eq. (28)]; as a result, we will obtain the collapsed state arising from the projective measurement at one particular output of a specific receiver's site.

In the following, we analyze the measurement results of received signals for three cases when the input signals are coherent, single-photon, and Poissonian mixed states.

A. Coherent states: Intensity operator

Theorem 2. Let the input signals of the QWDM network be coherent states. Then the intensity spectrum of the output signal related to the port jl, i.e., $I_{jl}(\omega) = {}^{(3)}_{\mathrm{C},jl}\langle\psi|\hat{a}_{j,l}^{\dagger(3)}(\omega)\hat{a}_{j,l}^{(3)}(\omega)|\psi\rangle_{\mathrm{C},jl}^{(3)}$, becomes

$$I_{jl}(\omega) \approx \begin{cases}\left|\sum_{i=1}^{N}\alpha_i \mathrm{G}_{ji}(\omega)\zeta_i(\omega)\right|^2, & |\omega-\omega_{ls}| \leqslant \Delta\omega_{\mathrm{A}}/2\\ 0 & \text{otherwise,}\end{cases}$$

where ω_{ls} is the central transmissible frequency with bandwidth $\Delta\omega_{\mathrm{A}}$ from input port s to output port l of the QR_j.

Proof. According to Eq. (27b) (Corollary 1), the state of the signal at the output port indicated by the mode of $\hat{a}_{j,l}^{(3)}$ in Fig. 2 is

$$|\psi\rangle_{\mathrm{C},jl}^{(3)} = \hat{D}\left(\sum_{i=1}^{N}\alpha_i\bar{\gamma}_{lsji}\right)|0\rangle^{(3)}. \tag{30}$$

Thus, the intensity related to the mode of $\hat{a}_{jl}^{(3)}(\omega)$ which is detected by QD_j at the jth receiver's site corresponding to the lth output port of QR_j is calculated as

$$\begin{aligned}I_{jl}(\omega) &= {}^{(3)}_{\mathrm{C},jl}\langle\psi|\hat{a}_{j,l}^{\dagger(3)}(\omega)\hat{a}_{j,l}^{(3)}(\omega)|\psi\rangle_{\mathrm{C},jl}^{(3)}\\ &= \left|\hat{a}_{j,l}^{(3)}(\omega)|\psi\rangle_{\mathrm{C},jl}^{(3)}\right|^2\\ &= \left|\sum_{i=1}^{N}\alpha_i\mathrm{G}_{ji}(\zeta_i)\mathrm{QR}_{j,ls}(\eta_{ji})\gamma_{lsji}(\omega)\right|^2\\ &= \left|\sum_{i=1}^{N}\alpha_i\mathrm{QR}_{j,ls}(\omega)\mathrm{G}_{ji}(\omega)\zeta_i(\omega)\right|^2.\end{aligned} \tag{31}$$

To derive Eq. (31), Eq. (24), as well as the relation

$$\hat{D}^{\dagger}(\alpha_i\bar{\gamma}_{lsji})\hat{a}_{j,l}^{(3)}(\omega)\hat{D}(\alpha_i\bar{\gamma}_{lsji}) = \hat{a}_{j,l}^{(3)}(\omega) + \alpha_i\bar{\gamma}_{lsji}(\omega),$$

is utilized. Since quantum receivers are demultiplexers or filters, a specific carrier frequency (wavelength) with the frequency band $\Delta\omega_{\mathrm{A}}$ is allowed to exit from each output port according to the input port number. Therefore, the frequency dependency of elements of $\underline{\mathrm{QR}}_j$ are approximated as

$$|\mathrm{QR}_{j,ls}(\omega)|^2 \approx \begin{cases} 1, & |\omega - \omega_{ls}| \leqslant \Delta\omega_{\mathrm{A}}/2 \\ 0 & \text{otherwise.} \end{cases} \tag{32}$$

The frequency band associated with central frequency ω_{ls} specifies the transmissible frequencies where the signal is inserted into input port s of the quantum receiver from output port j of the wavelength distributor and exits from output port l of QR_j (see Fig. 2). As a result, Eq. (31) for the transmissible frequency ω_{ls} is approximated by

$$I_{jl}(\omega_{ls}) \approx \left| \sum_{i=1}^{N} \alpha_i \mathrm{G}_{ji}(\omega_{ls}) \zeta_i(\omega_{ls}) \right|^2, \tag{33}$$

which shows the receiver indicated by $j \in \{1, \dots, N\}$ gains the ith user's information, i.e., $\zeta_i(\omega_{ls})$, from the lth output of the QR_j.

In demultiplexers, crosstalk effects are essential sources of noise that need to be considered. In practice, a narrow-band filter can diminish the crosstalk effects, e.g., the out-of-band crosstalk in each output of the quantum receiver. Furthermore, the quantum receiver output channels must be adequately frequency separated to eliminate in-band crosstalk. Preparing the signal with the narrow-band spectrum mitigates the in-band crosstalk for the transmitted signals that are distinguishable only by their frequency contents. It was shown in Ref. [34] that for weak quantum signals, noises caused by the crosstalk at outputs of AWGs as demultiplexers are in the same order of magnitude as the commercial dark count noise of the single-photon detectors, hence diminishing the degrading effects of the crosstalk in such networks.

B. Single-photon states: Projective measurement operator

Where the transmitters emit single-photon states, we analyze the output signal through a projective measurement since the local state related to each output port becomes a mixed state.

Definition. The projector operator $\hat{P}_{jl}(\omega_{ls})$ is defined as

$$\begin{aligned} \hat{P}_{jl}(\omega_{ls}) &= |1_{jl}(\omega_{ls})\rangle^{(3)}\,{}^{(3)}\langle 1_{jl}(\omega_{ls})| \\ &= \hat{a}^{\dagger(3)}_{j,l}(\omega_{ls})|0_{jl}(\omega_{ls})\rangle^{(3)}\,{}^{(3)}\langle 0_{jl}(\omega_{ls})|\hat{a}^{(3)}_{j,l}(\omega_{ls}), \end{aligned}$$

where $|1_{jl}(\omega_{ls})\rangle^{(3)}$ is the single-photon state produced by acting creation mode $\hat{a}^{\dagger(3)}_{j,l}(\omega_{ls})$ on the related vacuum state $|0_{jl}(\omega_{ls})\rangle^{(3)}$. Empirically, this projective measurement can be realized by detecting a single photon preceded by a ω_{ls} frequency filter placed at the output port number l of the jth quantum receiver.

Theorem 3. Let the input signals of the QWDM network be single-photon states. Then the collapsed state after the projective measurement $\hat{P}_{jl}(\omega_{ls})$ on $|\psi\rangle^{(3)}_{\mathrm{S}}$ [see Eq. (29)] becomes

$$\hat{P}_{jl}(\omega_{ls})|\psi\rangle^{(3)}_{\mathrm{S}} = |1_{jl}(\omega_{ls})\rangle^{(3)} \sum_{i=1}^{N} \left\{ \bar{\gamma}_{lsji}(\omega_{ls}) \prod_{i'\neq i} \times \sum_{(j',l')\neq(j,l)} \mathcal{N}_{l'sj'i'} \hat{a}^{\dagger(3)}_{j',l',\gamma_{l'sj'i'}} \right\} |0\rangle^{(3)}. \tag{34}$$

Proof. The proof is given in Appendix E 1.

Further analysis of the result of this projective measurement needs to identify $\hat{\mathrm{G}}^{\dagger}$ and $\zeta_i(\omega)$. This equation states that whenever a single-photon detector is activated in the output port of mode $\hat{a}_{j,l}(\omega_{ls})$, other detectors corresponding to the same frequency ω_{ls} will never be triggered provided only one transmitter sends a signal containing ω_{ls}. This implies that only one receiver can receive information encoded in frequency ω_{ls} transmitted by the transmitter at any given time (sampling time). However, each receiver may gain information in ω_{ls} transmitted by the ith transmitter during the next run with a certain probability (see Appendix F 1).

C. Poissonian mixed states: Projective measurement

In some applications, the Poissonian mixed state with a mean photon number much less than one ($|\alpha_i|^2 \ll 1$) can be a practical alternative for single-photon sources [49].

Theorem 4. Let the input signals of the QWDM network be Poissonian mixed states. Then the collapsed state in stage 3 after projective measurement $\hat{P}_{jl}(\omega_{ls})$ on $\rho^{(3)}_{\mathrm{C}}$ [see Eq. (28)] becomes

$$\begin{aligned} &\hat{P}_{jl}(\omega_{ls})\rho^{(3)}_{\mathrm{C}}\hat{P}_{jl}(\omega_{ls}) \\ &= |1_{jl}(\omega_{ls})\rangle^{(3)}\,{}^{(3)}\langle 1_{jl}(\omega_{ls})| \int \left(\prod_{i=1}^{N} \frac{d\phi_i}{2\pi}\right) e^{-|c_{lsj}|^2} |c_{lsj}\beta_{lsj} \\ &\quad \times (\omega_{ls})|^2 \prod_{i=1}^{N} \prod_{\substack{j'=1,l'=1 \\ (j',l')\neq(j,l)}}^{N,L} \hat{D}(\alpha_i \bar{\gamma}_{l'sj'i})|0\rangle^{(3)}\,{}^{(3)}\langle 0|\hat{D}^{\dagger}(\alpha_i \bar{\gamma}_{l'sj'i}), \end{aligned} \tag{35}$$

where $\beta_{lsj}(\omega)$ is a normalized wave packet, i.e., $\int |\beta_{lsj}(\omega)|^2 d\omega = 1$, and c_{lsj} is the norm of $\sum_{i=1}^{N} \alpha_i \bar{\gamma}_{lsji}(\omega)$.

Proof. The proof is given in Appendix E 2.

It is worth noting that the signal with the same frequency ω_{ls} transmitted by the ith sender can also be detected in the site of other receivers ($j' \neq j$). Therefore, more than one receiver can access the information transmitted by the ith transmitter. In other words, information leakage occurs when random-phased weak coherent states are used instead of single-photon sources (see Appendix F 2). For example, in QKD protocols, decoy states are utilized to overcome this difficulty [49].

D. Comparison of the measurement results for various input quantum signals

Although the complete comparison between the measurement results related to various inputs (coherent states, single-photon states, and Poissonian mixed states) requires the indication of the exact form of deployed network topology, we can still compare the measurement results of each kind of input quantum signal.

According to Eqs. (33) (Theorem 2), (34) (Theorem 3), and (35) (Theorem 4), the detection rate mainly depends on the factors γ_{lsji}. These factors are determined based on the specific WDM devices in the network. For instance, in the Lambdanet topology, the matrix $\underline{\mathrm{G}}$ as the mathematical representation of a star coupler with the matrix elements $|\mathrm{G}_{ji}| \approx \frac{1}{\sqrt{N}}$ [18] limits the number of users for a specific rate [58].

However, as expected, the weak coherent states and Poissonian mixed states have another critical factor, i.e., α_i. For these weak signals, since α_i is less than one, the detection rates of these two states are lower than in single-photon states [59].

As discussed before, the effects of losses and noises can be modeled via additional degrees of freedom [34,60]. These extra modes can lead to information leakage from all three input types. Moreover, vacuum fluctuation arising from these extra modes affects the quality of the signal, for instance, in homodyne detection [50]. Besides, entangling the actual receivers' outputs with these ambient modes [see Eq. (34)] reduces the coherency of the signals [61–63]. Finally, the effects of crosstalk noise can also be considered via a better approximation than Eq. (32) [34].

VI. CONCLUSION

This paper presents a general structure for a wide range of WDM communication systems' topologies and applications. It mathematically models the general WDM system in purely all-quantum terms, i.e., QWDM. Furthermore, the quantum signal evolution is described in a global and unified approach for various quantum light sources such as coherent, single-photon, and Poissonian mixed states with arbitrary spectral wave-packet profiles.

We introduced three main all-quantum evolutionary stages, namely, signal preparation, distribution, and reception stages. In particular, we obtain a key result in representing the quantum light signals at the final stage as a function of any desired input quantum signals and arbitrary distribution and reception quantum operators. The unitary distribution and reception quantum operators can be used to model the common devices in QWDM, such as star couplers, wavelength routers, multiplexers, demultiplexers, and filters.

We consider two different schemes, intensity and projection measurement operators, to evaluate the information encoded on the quantum signal sent from each transmitter to the receivers. We observe potentially correlated output states for single-photon and Poissonian mixed-state inputs. Moreover, depending on a particular application and using single-photon input states, we can show highly entangled states at the receiver end.

Using our methodology and modeling in this paper, one can describe equally the output statistics of classical sources of light (such as coherent states) and quantum sources of light (such as single photons). We show that if one uses single-photon sources, the quantum correlations can appear at the outputs of the network depending upon the quantum wavelength distributor ($\underline{\mathrm{G}}$). For example, a quantum Lambdanet broadcasting communication system with a star coupler as its wavelength distributor entangles the input single-photon states, while an ideal router as a wavelength distributor of a router-based communication system guides uncorrelated input single-photon states to separate outputs without introducing any quantum correlation (entanglement). Furthermore, the received signals are separable for coherent-state inputs, and no quantum correlation exists regardless of choosing any distributor mentioned above.

Although the current work does not directly consider the effects of losses and noises on the output signals, these effects can be included using the methodologies and models presented in this paper. The unitary operators can comprise both the real network system parameters and spurious ambient modes. One can also analyze the noises arising from crosstalk effects, phase drifts, etc., by considering an actual model of the network elements (such as star couplers, array waveguide grating, and optical fibers).

The results of this paper can be applied to various advanced QWDM applications such as fiber-to-the-home, Lambdanet, and router-based systems.

APPENDIX A: DESCRIPTION OF VARIOUS CONVENTIONAL WDM NETWORKS

The most popular conventional WDM network topologies depicted by Fig. 1 are explained as follows. In the long-haul fiber link network [Fig. 1(a)], the optical signal emitted by, e.g., a narrow-band laser source specified by the wavelength λ_i from the ith transmitter (Tx i) multiplexes with other emitted signals, and the multiplexed signals are transmitted via a common fiber link. A wavelength demultiplexer near the receivers separates signals and guides them toward the related receiver (Rx i) [7]. In a passive photonic loop access network [Fig. 1(b)], a central office is responsible for establishing communication between home users via sending and receiving specific signals by wavelength multiplexing and demultiplexing signals, respectively. A common fiber link between the central office and a remote node near the users is in charge of this communication. The remote node multiplexes the transmitted signals from users and demultiplexes the received signals from the central office. For instance, the first user receives a signal that is indicated by wavelength λ_1 and sends a signal that is indicated by wavelength λ_{N+1}. At the same time, the central office receives the signal indicated by wavelength λ_{N+1} and sends a signal indicated by wavelength λ_1 to the first user [7]. Lambdanet [Fig. 1(c)] is a fully connected network that can be utilized as an access network. Each node (user) in this topology has a transmitter emitting a specific wavelength. Each user's receiver can demultiplex and identify all the wavelengths used by all users. A star coupler distributes each signal equally to all users. Therefore, every user fully connects to others [6].

APPENDIX B: CREATION MODE EVOLUTION THROUGH THE WAVELENGTH DISTRIBUTOR

Using our paper indexing and terminology, we provide a review of quantum input-output relations in optical devices. Some textbooks and journal papers have addressed these relations, such as Refs. [18,38,64].

Any generic lossless passive quantum wavelength distributor depicted in Fig. 2 can be described by a frequency-dependent $N \times N$ linear matrix, $\underline{\mathrm{G}}(\omega)$. The field linear transform matrix $\underline{\mathrm{G}}$ relates the output annihilation modes of the frequency ω to input annihilation modes of the frequency ω as follows [64]:

$$\vec{\hat{a}}^{(2)}(\omega) \equiv \underline{\mathrm{G}}(\omega)\, \vec{\hat{a}}^{(1)}(\omega), \tag{B1}$$

where $\vec{\hat{a}}^{(\mathrm{s})}(\omega) = (\hat{a}_1^{(\mathrm{s})}(\omega), \ldots, \hat{a}_N^{(\mathrm{s})}(\omega))^{\mathrm{T}}, \quad \mathrm{s} \in \{1, 2\}$. Superscript T stands for transpose. As illustrated in Fig. 4(a), i

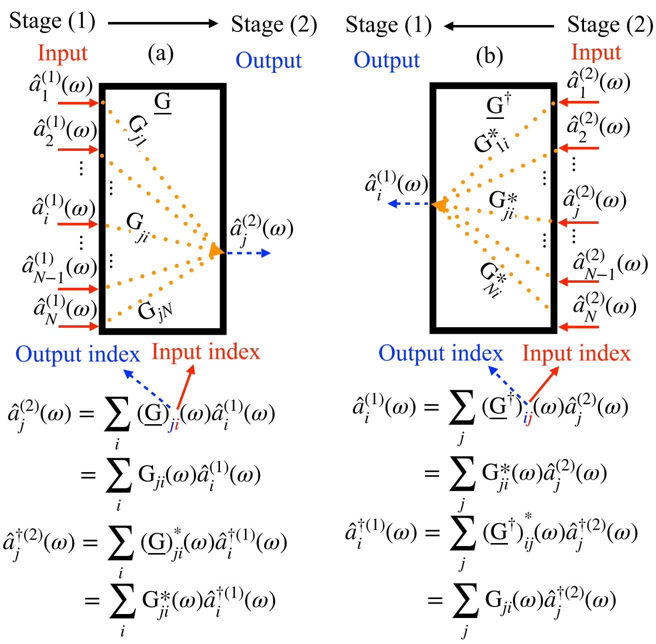

FIG. 4. Illustration of the distribution of field operators from the input (solid red line) of the general distributor to the specific output (blue dashed line) (a) from stage 1 to stage 2 and (b) vice versa. Note that $(\underline{\mathrm{G}}^{\dagger})_{ij} = \underline{\mathrm{G}}^{*}_{ji}$.

and j indices indicate the ith transmitter and the jth receiver, respectively. Therefore, the elementwise form of Eq. (B1) is rewritten as

$$\hat{a}_j^{(2)}(\omega) \equiv \sum_{i=1}^{N} (\underline{\mathrm{G}})_{ji}(\omega)\hat{a}_i^{(1)}(\omega) = \sum_{i=1}^{N} \mathrm{G}_{ji}(\omega)\hat{a}_i^{(1)}(\omega). \quad \text{(B2)}$$

In the Heisenberg picture, the field operator evolution can be described according to the unitary operator $\hat{\mathrm{G}}^{\dagger}$ as $\hat{a}_j^{(2)}(\omega) \xrightarrow{\hat{\mathrm{G}}^{\dagger}} \hat{\mathrm{G}}\,\hat{a}_j^{(2)}(\omega)\,\hat{\mathrm{G}}^{\dagger}$. Therefore,

$$\hat{a}_j^{(2)}(\omega) \xrightarrow{\hat{\mathrm{G}}^{\dagger}} \hat{\mathrm{G}}\,\hat{a}_j^{(2)}(\omega)\,\hat{\mathrm{G}}^{\dagger} = \sum_{i=1}^{N} \mathrm{G}_{ji}(\omega)\,\hat{a}_i^{(1)}(\omega). \quad \text{(B3)}$$

Due to the conservation of energy and reciprocity theorem, the matrix $\underline{\mathrm{G}}$ is unitary and symmetric at each frequency, respectively [36,56,65]. The unitarity of $\underline{\mathrm{G}}$ implies that $\underline{\mathrm{G}}(\omega)\,\underline{\mathrm{G}}^{\dagger}(\omega) = \underline{\mathrm{G}}^{\dagger}(\omega)\underline{\mathrm{G}}(\omega) = I$. Here we also use a dagger symbol (†) to denote matrix transpose conjugate, i.e., $\underline{\mathrm{G}}^{\dagger} = (\underline{\mathrm{G}}^{*})^{\mathrm{T}}$. Since the field transform matrix $\underline{\mathrm{G}}$ is a unitary matrix, one can write input modes of the frequency ω with respect to the output modes of the frequency ω by applying the conjugate transpose of the matrix $\underline{\mathrm{G}}$ from the left-hand side of Eq. (B1). Thus, as shown in Fig. 4(b),

$$\hat{a}_i^{(1)}(\omega) \equiv \sum_{j=1}^{N} (\underline{\mathrm{G}}^{\dagger})_{ij}(\omega)\hat{a}_j^{(2)}(\omega) = \sum_{j=1}^{N} \mathrm{G}^{*}_{ji}(\omega)\hat{a}_j^{(2)}(\omega). \quad \text{(B4)}$$

Equivalently, the unitary operator acting on the Hilbert space which relates input modes with respect to output modes is the inverse of $\hat{\mathrm{G}}^{\dagger}$, i.e., $\hat{\mathrm{G}}$ which gives rise to $\hat{a}_i^{(1)}(\omega) \xrightarrow{\hat{\mathrm{G}}} \hat{\mathrm{G}}^{\dagger}\,\hat{a}_i^{(1)}(\omega)\,\hat{\mathrm{G}}$. Thus,

$$\hat{a}_i^{(1)}(\omega) \xrightarrow{\hat{\mathrm{G}}} \hat{\mathrm{G}}^{\dagger}\hat{a}_i^{(1)}(\omega)\hat{\mathrm{G}} = \sum_{j=1}^{N} \mathrm{G}^{*}_{ji}(\omega)\,\hat{a}_j^{(2)}(\omega). \quad \text{(B5)}$$

Moreover, using the conjugate transpose of Eq. (B5), the matrix elements $[\mathrm{G}_{ji}]$, where j denotes the jth output and i denotes the ith input (see Fig. 2), relate the input creation modes of the frequency ω to the output as

$$\hat{a}_i^{\dagger(1)}(\omega) \xrightarrow{\hat{\mathrm{G}}} \hat{\mathrm{G}}^{\dagger}\hat{a}_i^{\dagger(1)}(\omega)\hat{\mathrm{G}} = \sum_{j=1}^{N} \mathrm{G}_{ji}(\omega)\,\hat{a}_j^{\dagger(2)}(\omega). \quad \text{(B6)}$$

APPENDIX C: RENORMALIZATION OF THE MODIFIED WAVE PACKET BY A WDM DISTRIBUTOR

The distributing operator $\hat{\mathrm{G}}$ transforms a photon wave-packet creation operator at input port i ($\hat{a}_{i,\zeta_i}^{\dagger(1)} = \int \zeta_i(\omega)\hat{a}_i^{\dagger(1)}(\omega)\,d\omega$) according to Eqs. (10) and (B6) as follows:

$$\begin{aligned}
\hat{\mathrm{G}}^{\dagger}\hat{a}_{i,\zeta_i}^{\dagger(1)}\hat{\mathrm{G}} &= \int \zeta_i(\omega)\sum_{j=1}^{N}\mathrm{G}_{ji}(\omega)\hat{a}_j^{\dagger(2)}(\omega)\,d\omega \\
&= \sum_{j=1}^{N}\int \zeta_i(\omega)\mathrm{G}_{ji}(\omega)\hat{a}_j^{\dagger(2)}(\omega)\,d\omega \\
&= \sum_{j=1}^{N}\sqrt{\int |\zeta_i(\omega')|^2|\mathrm{G}_{ji}(\omega')|^2\,d\omega'} \\
&\quad\times \int \frac{\zeta_i(\omega)\mathrm{G}_{ji}(\omega)}{\sqrt{\int |\zeta_i(\omega')|^2|\mathrm{G}_{ji}(\omega')|^2 d\omega'}}\hat{a}_j^{\dagger(2)}(\omega)\,d\omega.
\end{aligned} \quad \text{(C1)}$$

The integral term of the above equation in the last line is normalized and, therefore, can be considered as a single-photon wave-packet creation operator up to a global phase, e.g., the wave function $|\eta\rangle$ is physically equivalent to $e^{i\phi}|\eta\rangle$. Hence, we keep this global phase (degree of freedom) to define the single-photon wave function known as the photon wave packet. This degree of freedom allows us to determine the transformation on the input photon wave packet ζ_i as a unitary matrix with elements $\mathrm{G}_{ji}(\zeta_i)$, which becomes evident in the following. Inserting phase ϕ_{ij} ($e^{i\phi_{ji}}e^{-i\phi_{ji}} = 1$) in Eq. (C1) gives

$$\begin{aligned}
\hat{\mathrm{G}}^{\dagger}\hat{a}_{i,\zeta_i}^{\dagger(1)}\hat{\mathrm{G}} &= \sum_{j=1}^{N}\sqrt{\int |\zeta_i(\omega')|^2|\mathrm{G}_{ji}(\omega')|^2\,d\omega'}\,e^{i\phi_{ji}} \\
&\quad\times \int \frac{e^{-i\phi_{ji}}\zeta_i(\omega)\mathrm{G}_{ji}(\omega)}{\sqrt{\int |\zeta_i(\omega')|^2|\mathrm{G}_{ji}(\omega')|^2 d\omega'}}\hat{a}_j^{\dagger(2)}(\omega)\,d\omega \\
&= \sum_{j=1}^{N}\mathrm{G}_{ji}(\zeta_i)\int \eta_{ji}(\omega)\hat{a}_j^{\dagger(2)}(\omega)\,d\omega \\
&= \sum_{j=1}^{N}\mathrm{G}_{ji}(\zeta_i)\,\hat{a}_{j,\eta_{ji}}^{\dagger(2)},
\end{aligned} \quad \text{(C2)}$$

where the transformation amplitude $\mathrm{G}_{ji}(\zeta_i)$ and the output photon wave packet $\eta_{ji}(\omega)$ are defined as follows:

$$\mathrm{G}_{ji}(\zeta_i) = e^{i\phi_{ji}}\sqrt{\int |\zeta_i(\omega')|^2 |\mathrm{G}_{ji}(\omega')|^2\, d\omega'},$$
$$\eta_{ji}(\omega) = \frac{e^{-i\phi_{ji}}\zeta_i(\omega)\mathrm{G}_{ji}(\omega)}{\sqrt{\int |\zeta_i(\omega')|^2 |\mathrm{G}_{ji}(\omega')|^2\, d\omega'}}. \tag{C3}$$

Let us compare the transformation of operator $\hat{\mathrm{G}}$ on a generic photon wave packet ζ_i [Eq. (C2)] with its corresponding transformation on a single-frequency-mode photon [Eq. (10)]:

$$\hat{\mathrm{G}}^\dagger \hat{a}_i^{\dagger(1)}(\omega)\hat{\mathrm{G}} = \sum_{j=1}^{N} \mathrm{G}_{ji}(\omega)\, \hat{a}_j^{\dagger(2)}(\omega),$$
$$\hat{\mathrm{G}}^\dagger \hat{a}_{i,\zeta_i}^{\dagger(1)}\hat{\mathrm{G}} = \sum_{j=1}^{N} \mathrm{G}_{ji}(\zeta_i)\, \hat{a}_{j,\eta_{ji}}^{\dagger(2)}. \tag{C4}$$

As you see, the format of the above two equations is similar. The transform matrix $\underline{\mathrm{G}}(\omega)$ with elements $\mathrm{G}_{ji}(\omega)$ is the transform matrix for photons with frequency ω, while the transform matrix $\underline{\mathrm{G}}(\zeta_i)$ with elements $\mathrm{G}_{ji}(\zeta_i)$ is the transform matrix for photons with wave packet ζ_i. The main difference in the above two equations is that the device operator $\hat{\mathrm{G}}$ keeps the spectral shape (wave packet) of a single-frequency-mode photon $\hat{a}^\dagger(\omega)$. However, it changes the shape of the continuous-mode single photon $\hat{a}_{\zeta_i}^\dagger$ from input ζ_i at the input port i into η_{ji} at the output j.

To make the above two equations more comparable, we assume the distributor device's transform matrix elements $\mathrm{G}_{ji}(\omega)$ remain unchanged for the spectral width of the photon wave packet $\zeta_i(\omega)$. Therefore, we can approximate $\mathrm{G}_{ji}(\omega)\zeta_i(\omega)$ with $\mathrm{G}_{ji}(\omega_0)\zeta_i(\omega)$, where ω_0 is the central frequency of the photon wave packet $\zeta_i(\omega)$. Therefore, Eq. (C3) reduces to

$$\mathrm{G}_{ji}(\zeta_i) = e^{i\phi_{ji}}\sqrt{\int |\zeta_i(\omega')|^2 |\mathrm{G}_{ji}(\omega')|^2\, d\omega'}$$
$$= e^{i\phi_{ji}}\sqrt{|\mathrm{G}_{ji}(\omega_0)|^2 \int |\zeta_i(\omega')|^2\, d\omega'}$$
$$= e^{i\phi_{ji}}|\mathrm{G}_{ji}(\omega_0)|,$$
$$\eta_{ji}(\omega) = \frac{e^{-i\phi_{ji}}\zeta_i(\omega)\mathrm{G}_{ji}(\omega)}{\sqrt{\int |\zeta_i(\omega')|^2 |\mathrm{G}_{ji}(\omega')|^2\, d\omega'}}$$
$$= \frac{e^{-i\phi_{ji}}\zeta_i(\omega)\mathrm{G}_{ji}(\omega_0)}{\sqrt{|\mathrm{G}_{ji}(\omega_0)|^2 \int |\zeta_i(\omega')|^2\, d\omega'}}$$
$$= \frac{\zeta_i(\omega)\mathrm{G}_{ji}(\omega_0)}{e^{i\phi_{ji}}|\mathrm{G}_{ji}(\omega_0)|}. \tag{C5}$$

Let us assume the phase ϕ_{ji} equals the phase of $\mathrm{G}_{ji}(\omega_0)$, which makes Eq. (C5) as follows:

$$\mathrm{G}_{ji}(\zeta_i) = \mathrm{G}_{ji}(\omega_0), \quad \eta_{ji}(\omega) = \zeta_i(\omega). \tag{C6}$$

Therefore, Eqs. (C4) become completely equivalent:

$$\hat{\mathrm{G}}^\dagger \hat{a}_i^{\dagger(1)}(\omega)\hat{\mathrm{G}} = \sum_{j=1}^{N} \mathrm{G}_{ji}(\omega)\, \hat{a}_j^{\dagger(2)}(\omega),$$
$$\hat{\mathrm{G}}^\dagger \hat{a}_{i,\zeta_i}^{\dagger(1)}\hat{\mathrm{G}} = \sum_{j=1}^{N} \mathrm{G}_{ji}(\zeta_i)\, \hat{a}_{j,\eta_{ji}}^{\dagger(2)} = \sum_{j=1}^{N} \mathrm{G}_{ji}(\omega_0)\, \hat{a}_{j,\zeta_i}^{\dagger(2)}, \tag{C7}$$

where both equations do not change the photon wave-packet ζ_i representation from the input to the output ports.

1. Single frequency mode: $|\zeta(\omega)|^2 = \delta(\omega - \omega_0)$

The photon wave packet of a single-mode photon with frequency ω_0 is defined as $|\zeta_i(\omega)|^2 = \delta(\omega - \omega_0)$. For such a photon wave packet the transform matrix elements $\mathrm{G}_{ji}(\zeta_i)$ [Eq. (C5)] reduce to

$$\mathrm{G}_{ji}(\zeta_i) = e^{i\phi_{ji}}\sqrt{\int |\zeta_i(\omega)|^2 |\mathrm{G}_{ji}(\omega)|^2\, d\omega}$$
$$= e^{i\phi_{ji}}\sqrt{\int \delta(\omega - \omega_0) |\mathrm{G}_{ji}(\omega)|^2\, d\omega} = \mathrm{G}_{ji}(\omega_0), \tag{C8}$$

where we have assumed the phase ϕ_{ji} equals the phase of $\mathrm{G}_{ji}(\omega_0)$, i.e., $\mathrm{G}_{ji}(\omega_0) = e^{i\phi_{ji}}|\mathrm{G}_{ji}(\omega_0)|$. Therefore, $\mathrm{G}_{ji}(\zeta_i)$ is the extension of $\mathrm{G}_{ji}(\omega)$ for photon wave packet ζ_i.

APPENDIX D: QUANTUM RECEIVERS FOR QWDM COMMUNICATION SYSTEMS

In the language of WDM, $\underline{\mathrm{QR}}_j$ is a wavelength demultiplexer or a filter. In the context of QWDM, these devices are modeled by unitary L input and L output quantum demultiplexers for separating the different wavelengths inserted in one input port of $\underline{\mathrm{QR}}_j$ to specific output ports, which depends on frequency assignments. Input and output port numbers are labeled by s and l indices. The transmissible frequency ω_{ls} of $\underline{\mathrm{QR}}_j$ relates the sth input to the lth output, respectively. Since only one of the input ports is fed by the jth output of $\underline{\mathrm{G}}$, vacuum states feed the other input ports. In other words, a quantum demultiplexer can be realized by an $L \times L$ router wherein only one of its inputs is used. For instance, in an arrayed-waveguide-grating-based quantum demultiplexer, the relation between ω_{ls} and its related wavelength is $\omega_{ls} = 2\pi c/\lambda_{l-s+1\,\mathrm{mod}L}$ [7,34]. Therefore, we supply the creation mode from output j of $\underline{\mathrm{G}}$ related to each input of $\underline{\mathrm{QR}}_j$ with an additional subindex s corresponding to the input index of the receiver device as $\hat{a}_{j,s}^{\dagger(2)}(\omega)$. It is important to note that $\hat{a}_j^{\dagger(2)}(\omega) \equiv \hat{a}_{j,s}^{\dagger(2)}(\omega)$ for the arbitrary input $s \in \{1, \ldots, L\}$ of $\underline{\mathrm{QR}}_j$ that our model chooses to feed. For example, Fig. 5 illustrates a 3×3 quantum receiver for two different users, j and j'. In this paper, as shown in Fig. 2, the jth quantum receiver's site is defined as a combination of output j of $\underline{\mathrm{G}}$, the quantum demultiplexer or filter $\underline{\mathrm{QR}}_j$, followed by their corresponding photodetectors. In Figs. 5(a) and 5(b), we assume the output port of the wavelength distributor of the communication system goes to the port labeled $s = 1$ of the jth receiver and $s = 2$

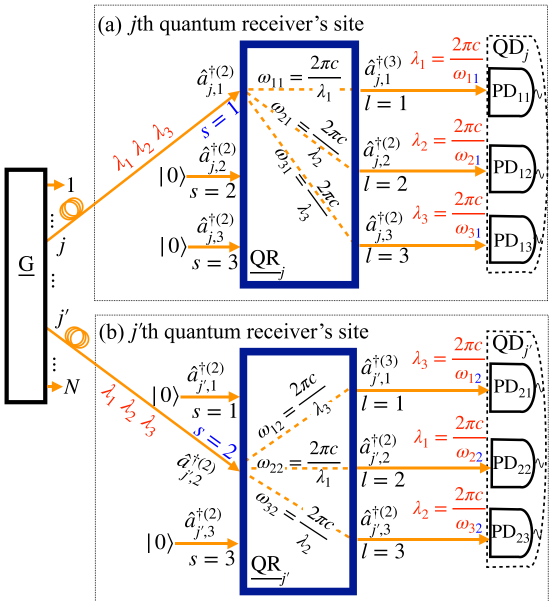

FIG. 5. Schematic of a router-based model of a 3×3 $\underline{\mathrm{QR}}_j$ utilized in QWDM. Input port number is fixed to (a) $s=1$ and (b) $s=2$.

of the j'th receiver, respectively. Assume a communication system with three different wavelengths, i.e., $K=3$ and from $L\geqslant \min\{k+1,K\}$ the number of the input-output port of both receivers' quantum demultiplexers can be $L=3$. Thus, all three wavelengths supported by the communication system are accessible to both receivers' sites j and j'. However, the order of the received wavelengths with respect to the output labels of various receiver devices is different. Consider the same input port number for both quantum demultiplexers, e.g., $s=1$ for j and j'. Thus, the same wavelength will exit from the output port number l of both demultiplexers, provided $\underline{\mathrm{QR}}_j$ and $\underline{\mathrm{QR}}'_j$ are identical devices. Note that if the devices are not identical in a very general case, the frequency ω_{ls} exited from the lth output of different demultiplexers is not necessarily the same. This frequency is determined based on the information from the device's catalog. Having said that, by proper rearrangement of the output port numbers, we assume that the frequency ordering of our quantum model for every $\underline{\mathrm{QR}}_j$ is the same; i.e., the ω_{ls} corresponding to $\underline{\mathrm{QR}}_j$ $\forall j\in\{1,\dots,N\}$ is identified by a similar wavelength. Consequently, using the same input label, s, does not compromise the generality of our model. We emphasize that in this paper, the quantum model of $\underline{\mathrm{QR}}_j$ is an $L\times L$ demultiplexer (quantum router), where L, the dimension of $\underline{\mathrm{QR}}_j$, equals K, the maximum number of wavelengths used in the communication system, i.e., $L=K$.

APPENDIX E: MATHEMATICAL DETAILS OF PROJECTIVE MEASUREMENT ON THE EVOLVED SINGLE-PHOTON AND POISSONIAN MIXED STATES

1. Single-photon states

To derive Eq. (34) (Theorem 3), first note that for an arbitrary mode $\hat{a}_i(\omega)$

$$\begin{aligned}\hat{a}_i(\omega)\hat{a}^\dagger_j(\omega')|0\rangle &= [\delta_{ij}\delta(\omega-\omega')+\hat{a}^\dagger_j(\omega')\hat{a}_i(\omega)]|0\rangle\\ &= \delta_{ij}\delta(\omega-\omega')|0\rangle = [\hat{a}_i(\omega),\hat{a}^\dagger_j(\omega')]|0\rangle,\end{aligned}\tag{E1}$$

where $[\hat{a}_i(\omega),\hat{a}^\dagger_j(\omega')]=\delta_{ij}\delta(\omega-\omega')$. Then, using Eq. (19), the following equation is deduced:

$$\hat{a}^{(3)}_{j,l}(\omega_{ls})\hat{a}^{\dagger(3)}_{j',l',\gamma_{l'sj'i}}|0\rangle^{(3)} = \big[\hat{a}^{(3)}_{j,l}(\omega_{ls}),\hat{a}^{\dagger(3)}_{j',l',\gamma_{l'sj'i}}\big]|0\rangle^{(3)},\tag{E2}$$

where (also see Ref. [18])

$$\begin{aligned}\big[\hat{a}^{(3)}_{j,l}(\omega_{ls}),\hat{a}^{\dagger(3)}_{j',l',\gamma_{l'sj'i}}\big] &= \int d\omega\gamma_{l'sj'i}(\omega)\big[\hat{a}^{(3)}_{j,l}(\omega_{ls}),\hat{a}^{\dagger(3)}_{j',l'}(\omega_{l's})\big]\\ &= \int d\omega\gamma_{l'sj'i}(\omega)\delta(\omega_{ls}-\omega_{l's})\delta_{jj'}\delta_{ll'}\\ &= \gamma_{lsji}(\omega_{ls})\delta_{jj'}\delta_{ll'}.\end{aligned}\tag{E3}$$

Furthermore, from Eq. (E3), the following relation is obtained:

$$\begin{aligned}&\hat{a}^{(3)}_{j,l}(\omega_{ls})\sum_{j'l'}\mathcal{N}_{l'sj'i}\hat{a}^{\dagger(3)}_{j',l',\gamma_{l'sj'i}}\\ &\quad=\bar{\gamma}_{lsji}(\omega_{ls})+\sum_{j'l'}\mathcal{N}_{l'sj'i}\hat{a}^{\dagger(3)}_{j',l',\gamma_{l'sj'i}}\hat{a}^{(3)}_{j,l}(\omega_{ls}),\end{aligned}\tag{E4}$$

where $\bar{\gamma}_{lsji}$ is defined in Eq. (24). By recursive use of Eqs. (E2) and (E4), the action of $\hat{P}_{jl}(\omega_{ls})$ on $|\psi\rangle^{(3)}_{\mathrm{S}}$ is obtained via transporting the annihilation operator $\hat{a}^{(3)}_{j,l}(\omega_{ls})$ to the right-hand side of creation operators $\hat{a}^{\dagger(3)}_{j',l',\gamma_{l'sj'i}}$ according to the commutation relation between these operators [Eq. (E3)]. Therefore, the following result is acquired:

$$\begin{aligned}\hat{P}_{jl}(\omega_{ls})|\psi\rangle^{(3)}_{\mathrm{S}} &= \hat{a}^{\dagger(3)}_{j,l}(\omega_{ls})|0_{jl}(\omega_{ls})\rangle^{(3)}\,{}^{(3)}\langle 0_{jl}(\omega_{ls})|\hat{a}^{(3)}_{j,l}(\omega_{ls})\prod_{i'}\sum_{j'l'}\mathcal{N}_{l'sj'i'}\hat{a}^{\dagger(3)}_{j',l',\gamma_{l'sj'i'}}|0\rangle^{(3)}\\ &= |1_{jl}(\omega_{ls})\rangle^{(3)}\langle 0_{jl}(\omega_{ls})|\sum_{j'l'}\mathcal{N}_{l'sj'1}\hat{a}^{(3)}_{j,l}(\omega_{ls})\hat{a}^{\dagger(3)}_{j',l',\gamma_{l'sj'1}}\prod_{i'\neq 1}\sum_{j'l'}\mathcal{N}_{l'sj'i'}\hat{a}^{\dagger(3)}_{j',l',\gamma_{l'sj'i'}}|0\rangle^{(3)}\\ &= |1_{jl}(\omega_{ls})\rangle^{(3)}\langle 0_{jl}(\omega_{ls})|\left\{\bar{\gamma}_{lsj1}(\omega_{ls})+\sum_{j'l'}\mathcal{N}_{l'sj'1}\hat{a}^{\dagger(3)}_{j',l',\gamma_{l'sj'1}}\hat{a}^{(3)}_{j,l}(\omega_{ls})\right\}\sum_{j'l'}\mathcal{N}_{l'sj'2}\hat{a}^{\dagger(3)}_{j',l',\gamma_{l'sj'2}}\prod_{i'\neq 1,2}\\ &\quad\times\sum_{j'l'}\mathcal{N}_{l'sj'i'}\hat{a}^{\dagger(3)}_{j',l',\gamma_{l'sj'i'}}|0\rangle^{(3)}\end{aligned}$$

$$
\begin{aligned}
&= |1_{jl}(\omega_{ls})\rangle^{(3)}\langle 0_{jl}(\omega_{ls})| \Bigg\{ \bar{\gamma}_{lsj1}(\omega_{ls}) \sum_{j'l'} \mathcal{N}_{l'sj'2} \hat{a}^{\dagger(3)}_{j',l',\gamma_{l'sj'2}} + \bar{\gamma}_{lsj2}(\omega_{ls}) \sum_{j'l'} \mathcal{N}_{l'sj'1} \hat{a}^{\dagger(3)}_{j',l',\gamma_{l'sj'1}} \\
&\quad + \sum_{j'l'} \mathcal{N}_{l'sj'1} \hat{a}^{\dagger(3)}_{j',l',\gamma_{l'sj'1}} \sum_{j'l'} \mathcal{N}_{l'sj'2} \hat{a}^{\dagger(3)}_{j',l',\gamma_{l'sj'2}} \hat{a}^{(3)}_{j,l}(\omega_{ls}) \Bigg\} \prod_{i'\neq 1,2} \sum_{j'l'} \mathcal{N}_{l'sj'i'} \hat{a}^{\dagger(3)}_{j',l',\gamma_{l'sj'i'}} |0\rangle^{(3)} \\
&= |1_{jl}(\omega_{ls})\rangle^{(3)} \Bigg\{ \bar{\gamma}_{lsj1}(\omega_{ls}) \prod_{i'\neq 1} \sum_{(j',l')\neq(j,l)} \mathcal{N}_{l'sj'i'} \hat{a}^{\dagger(3)}_{j',l',\gamma_{l'sj'i'}} + \bar{\gamma}_{lsj2}(\omega_{ls}) \prod_{i'\neq 2} \sum_{(j',l')\neq(j,l)} \mathcal{N}_{l'sj'i'} \hat{a}^{\dagger(3)}_{j',l',\gamma_{l'sj'i'}} + \cdots \\
&\quad + \bar{\gamma}_{lsjN}(\omega_{ls}) \prod_{i'\neq N} \sum_{(j',l')\neq(j,l)} \mathcal{N}_{l'sj'i'} \hat{a}^{\dagger(3)}_{j',l',\gamma_{l'sj'i'}} \Bigg\} |0\rangle^{(3)} \\
&= |1_{jl}(\omega_{ls})\rangle^{(3)} \sum_{i=1}^{N} \Bigg\{ \bar{\gamma}_{lsji}(\omega_{ls}) \prod_{i'\neq i} \sum_{(j',l')\neq(j,l)} \mathcal{N}_{l'sj'i'} \hat{a}^{\dagger(3)}_{j',l',\gamma_{l'sj'i'}} \Bigg\} |0\rangle^{(3)}. \qquad \text{(E5)}
\end{aligned}
$$

Since $\langle 0_{jl}(\omega_{ls})|\hat{a}^{\dagger(3)}_{j,l}(\omega_{ls}) = 0$, there remains no term related to the mode $\hat{a}^{\dagger(3)}_{j,l}(\omega_{ls})$ in the last line brackets.

2. Poissonian mixed states

According to the material of Sec. IV B, Eq. (28) gives the evolved Poissonian mixed states to stage 3, i.e., $\rho^{(3)}_{\mathrm{C}}$. Moreover, in Sec. V C, the action of projective operator $\hat{P}_{jl}(\omega_{ls})$ on $\rho^{(3)}_{\mathrm{C}}$ gives rise to Eq. (35) (Theorem 4). Here, we elucidate the details of the mathematical procedure leading to the final result of Eq. (35) (Theorem 4) as

$$
\begin{aligned}
\hat{P}_{jl}(\omega_{ls})\rho^{(3)}_{\mathrm{C}}\hat{P}_{jl}(\omega_{ls}) &= |1_{jl}(\omega_{ls})\rangle^{(3)}\,{}^{(3)}\langle 1_{jl}(\omega_{ls})| \times \int \left(\prod_{i=1}^{N}\frac{d\phi_i}{2\pi}\right) {}^{(3)}\langle 1_{jl}(\omega_{ls})| \left\{ \prod_{i=1}^{N} \hat{D}(\alpha_i\bar{\gamma}_{lsji})|0\rangle^{(3)}\,{}^{(3)}\langle 0|\hat{D}^{\dagger}(\alpha_i\bar{\gamma}_{lsji}) \right\} |1_{jl}(\omega_{ls})\rangle^{(3)} \\
&\quad \times \prod_{i=1}^{N} \prod_{(j',l')\neq(j,l)}^{N,L} \hat{D}(\alpha_i\bar{\gamma}_{l'sj'i})|0\rangle^{(3)}\,{}^{(3)}\langle 0|\hat{D}^{\dagger}(\alpha_i\bar{\gamma}_{l'sj'i}) \\
&= |1_{jl}(\omega_{ls})\rangle^{(3)}\,{}^{(3)}\langle 1_{jl}(\omega_{ls})| \int \left(\prod_{i=1}^{N}\frac{d\phi_i}{2\pi}\right) {}^{(3)}\langle 1_{jl}(\omega_{ls})|\hat{D}\left(\sum_{i=1}^{N}\alpha_i\bar{\gamma}_{lsji}\right)|0\rangle^{(3)}\,{}^{(3)}\langle 0|\hat{D}^{\dagger}\left(\sum_{i=1}^{N}\alpha_i\bar{\gamma}_{lsji}\right)|1_{jl} \\
&\quad \times (\omega_{ls})\rangle^{(3)} \prod_{i=1}^{N} \prod_{(j',l')\neq(j,l)}^{N,L} \hat{D}(\alpha_i\bar{\gamma}_{l'sj'i})|0\rangle^{(3)}\,{}^{(3)}\langle 0|\hat{D}^{\dagger}(\alpha_i\bar{\gamma}_{l'sj'i}) \\
&= |1_{jl}(\omega_{ls})\rangle^{(3)}\,{}^{(3)}\langle 1_{jl}(\omega_{ls})| \int \left(\prod_{i=1}^{N}\frac{d\phi_i}{2\pi}\right) e^{-|c_{lsj}|^2}|c_{lsj}\beta_{lsj}(\omega_{ls})|^2 \prod_{i=1}^{N} \prod_{(j',l')\neq(j,l)}^{N,L} \hat{D}(\alpha_i\bar{\gamma}_{l'sj'i})|0\rangle^{(3)}\,{}^{(3)}\langle 0| \\
&\quad \times \hat{D}^{\dagger}(\alpha_i\bar{\gamma}_{l'sj'i}), \qquad \text{(E6)}
\end{aligned}
$$

where $c_{lsj}\beta_{lsj}(\omega) = \sum_{i=1}^{N}\alpha_i\bar{\gamma}_{lsji}(\omega)$. As also mentioned in Sec. V C, $\beta_{lsj}(\omega)$ is a normalized wave packet, and c_{lsj} is the norm of $\sum_{i=1}^{N}\alpha_i\bar{\gamma}_{lsji}(\omega)$. To obtain the last line of Eq. (E6), the following relation is used:

$$
\begin{aligned}
&{}^{(3)}\langle 1_{jl}(\omega_{ls})|\hat{D}\left(\sum_{i=1}^{N}\alpha_i\bar{\gamma}_{lsji}\right)|0\rangle^{(3)} \\
&={}^{(3)}\langle 1_{jl}(\omega_{ls})|\hat{D}(c_{lsj}\beta_{lsj}(\omega))|0\rangle^{(3)} = e^{-|c_{lsj}|^2/2}c_{lsj}\beta_{lsj}(\omega_{ls}), \qquad \text{(E7)}
\end{aligned}
$$

where

$$
\begin{aligned}
\hat{D}(c_{lsj}\beta_{lsj}(\omega))|0\rangle^{(3)} &= e^{-|c_{lsj}|^2/2}\sum_{n}\frac{c^n_{lsj}}{n!}\hat{a}^{\dagger(3)^n}_{j,l,\beta_{lsj}}|0\rangle^{(3)}, \\
\hat{a}^{\dagger(3)}_{j,l,\beta_{lsj}} &= \int \beta_{lsj}(\omega)\hat{a}^{\dagger(3)}_{j,l}(\omega)d\omega, \qquad \text{(E8)}
\end{aligned}
$$

and (see Eq. (E2) and Ref. [18])

$$
\begin{aligned}
{}^{(3)}\langle 1_{jl}(\omega_{ls})|\hat{a}^{\dagger(3)^n}_{j,l,\beta_{lsj}}|0\rangle^{(3)} &= {}^{(3)}\langle 0_{jl}(\omega_{ls})|[\hat{a}_{j,l}(\omega_{jl}),\hat{a}^{\dagger(3)^n}_{j,l,\beta_{lsj}}]|0\rangle^{(3)} \\
&= {}^{(3)}\langle 0_{jl}(\omega_{ls})|\hat{a}^{\dagger(3)^{n-1}}_{j,l,\beta_{lsj}} n\beta_{lsj}(\omega_{ls})|0\rangle^{(3)} \\
&= \delta_{1n}\beta_{lsj}(\omega_{ls}). \qquad \text{(E9)}
\end{aligned}
$$

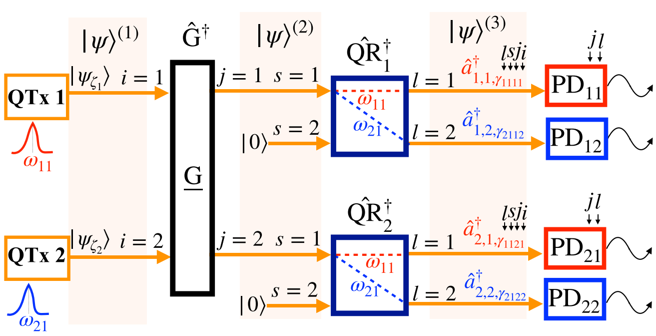

FIG. 6. Schematic configuration of a QWDM system for two transmitters and two receivers. QTx1 and QTx2 are two narrow-band sources with central frequencies ω_{11} and ω_{21}, respectively.

APPENDIX F: EXAMPLES OF QUANTUM SIGNAL MEASUREMENT IN QWDM COMMUNICATION SYSTEMS WITH TWO QUANTUM TRANSMITTERS AND TWO QUANTUM RECEIVERS

Figure 6 illustrates a generic QWDM system where the input-output number of the wavelength distributor $\underline{\mathrm{G}}$ and the quantum receivers $\underline{\mathrm{QR}}_j$ $j \in \{1, 2\}$ are $N = 2$ and $L = 2$, respectively. As mentioned previously, $\underline{\mathrm{QR}}_j$ is a demultiplexer that can be implemented by an AWG. The element $\mathrm{QR}_{j,11}(\omega)$ $[\mathrm{QR}_{j,21}(\omega)]$ has a narrow frequency band around the guided frequency ω_{11} (ω_{21}). For the sake of simplicity, we assume $\zeta_1(\omega)$ $[\zeta_2(\omega)]$ has a narrow-band spectrum with the central frequency ω_{11} (ω_{21}). Regardless of a physical model for $\underline{\mathrm{G}}$ (being a star coupler or an AWG), since $\zeta_1(\omega)$ $[\zeta_2(\omega)]$ and $\mathrm{QR}_{j,21}(\omega)$ $[\mathrm{QR}_{j,11}(\omega)]$ do not overlap [i.e., $\zeta_1(\omega)\mathrm{QR}_{j,21}(\omega) \approx 0$ and $\zeta_2(\omega)\mathrm{QR}_{j,11}(\omega) \approx 0$], one can consider the following approximation according to Eqs. (13a) and (20a) as $\gamma_{2111}(\omega) \approx 0$, $\gamma_{2121}(\omega) \approx 0$, $\gamma_{1112}(\omega) \approx 0$, and $\gamma_{1122}(\omega) \approx 0$.

1. Example for single-photon states: Projective measurement

Consider a single-photon state as the quantum state of each transmitted signal. Therefore, Eq. (29) for the particular QWDM system presented in Fig. 6 becomes

$$\begin{aligned}
|\psi\rangle_{\mathrm{S}}^{(3)} &= \prod_{i=1}^{2}\left(\sum_{j=1}^{2}\sum_{l=1}^{2}\mathcal{N}_{lsji}\hat{a}^{\dagger(3)}_{j,l,\gamma_{lsji}}\right)|0\rangle^{(3)} \\
&= \big(\mathcal{N}_{1111}\hat{a}^{\dagger(3)}_{1,1,\gamma_{1111}} + \mathcal{N}_{2111}\hat{a}^{\dagger(3)}_{1,2,\gamma_{2111}} + \mathcal{N}_{1121}\hat{a}^{\dagger(3)}_{2,1,\gamma_{2111}} \\
&\quad + \mathcal{N}_{2121}\hat{a}^{\dagger(3)}_{2,2,\gamma_{2121}}\big)\big(\mathcal{N}_{1112}\hat{a}^{\dagger(3)}_{1,1,\gamma_{1112}} + \mathcal{N}_{2112}\hat{a}^{\dagger(3)}_{1,2,\gamma_{2112}} \\
&\quad + \mathcal{N}_{1122}\hat{a}^{\dagger(3)}_{2,1,\gamma_{2112}} + \mathcal{N}_{2122}\hat{a}^{\dagger(3)}_{2,2,\gamma_{2122}}\big)|0\rangle^{(3)} \\
&\approx \big(\mathcal{N}_{1111}\hat{a}^{\dagger(3)}_{1,1,\gamma_{1111}} + \mathcal{N}_{1121}\hat{a}^{\dagger(3)}_{2,1,\gamma_{1121}}\big) \\
&\quad \times\big(\mathcal{N}_{2112}\hat{a}^{\dagger(3)}_{1,2,\gamma_{2112}} + \mathcal{N}_{2122}\hat{a}^{\dagger(3)}_{2,2,\gamma_{2122}}\big)|0\rangle^{(3)} \\
&= \mathcal{N}_{1111}\mathcal{N}_{2112}|1100\rangle^{(3)} + \mathcal{N}_{1111}\mathcal{N}_{2122}|1001\rangle^{(3)} \\
&\quad + \mathcal{N}_{1121}\mathcal{N}_{2112}|0110\rangle^{(3)} + \mathcal{N}_{1121}\mathcal{N}_{2122}|0011\rangle^{(3)},
\end{aligned} \tag{F1}$$

where $\hat{a}^{\dagger(3)}_{1,1,\gamma_{1111}}|0\rangle^{(3)} = |1000\rangle^{(3)}$, $\hat{a}^{\dagger(3)}_{1,2,\gamma_{2112}}|0\rangle^{(3)} = |0100\rangle^{(3)}$, $\hat{a}^{\dagger(3)}_{2,1,\gamma_{1121}}|0\rangle^{(3)} = |0010\rangle^{(3)}$, and $\hat{a}^{\dagger(3)}_{2,2,\gamma_{2122}}|0\rangle^{(3)} = |0001\rangle^{(3)}$ indicate the presence of a single photon at the outputs labeled by $(j, l) = (1, 1)$, $(j, l) = (1, 2)$, $(j, l) = (2, 1)$, and $(j, l) = (2, 2)$, respectively.

The projective measurement operator $\hat{P}_{11}(\omega_{11}) = |1_{11}(\omega_{11})\rangle^{(3)}\,{}^{(3)}\langle 1_{11}(\omega_{11})|$ performed on Eq. (F1) yields

$$\begin{aligned}
\hat{P}_{11}(\omega_{11})|\psi\rangle_{\mathrm{S}}^{(3)} &= \mathcal{N}_{1111}\mathcal{N}_{2112}\,{}^{(3)}\langle 1_{11}(\omega_{11})|1100\rangle^{(3)} \\
&\quad + \mathcal{N}_{1111}\mathcal{N}_{2122}\,{}^{(3)}\langle 1_{11}(\omega_{11})|1001\rangle^{(3)}.
\end{aligned} \tag{F2}$$

Equation (F2) is simplified with the help of

$${}^{(3)}\langle 1_{11}(\omega_{11})|1100\rangle^{(3)} = \gamma_{1111}|100\rangle^{(3)}, \tag{F3}$$

$${}^{(3)}\langle 1_{11}(\omega_{11})|1001\rangle^{(3)} = \gamma_{1111}|001\rangle^{(3)}, \tag{F4}$$

in which, using Eqs. (E2) and (E3), we utilize the following relation:

$$\begin{aligned}
{}^{(3)}\langle 1_{11}(\omega_{11})|1\rangle^{(3)} &= {}^{(3)}\langle 0_{11}(\omega_{11})|\hat{a}^{(3)}_{1,1}(\omega_{11})\hat{a}^{\dagger(3)}_{1,1,\gamma_{1111}}|0\rangle^{(3)} \\
&= \gamma_{1111}.
\end{aligned} \tag{F5}$$

As a result, the collapsed state of Eq. (F1) due to the projective measurement, up to a global phase, is

$$\begin{aligned}
\frac{\hat{P}_{11}(\omega_{11})|\psi\rangle_{\mathrm{S}}^{(3)}}{\sqrt{{}^{(3)}_{\mathrm{S}}\langle\psi|\hat{P}^2_{11}(\omega_{11})|\psi\rangle^{(3)}_{\mathrm{S}}}} &= \frac{1}{\sqrt{\mathcal{N}^2_{2112} + \mathcal{N}^2_{2122}}}|1_{11}(\omega_{11})\rangle^{(3)} \\
&\quad \times\{\mathcal{N}_{2112}|100\rangle^{(3)} + \mathcal{N}_{2122}|001\rangle^{(3)}\},
\end{aligned} \tag{F6}$$

where ${}^{(3)}_{\mathrm{S}}\langle\psi|\hat{P}^2_{11}(\omega_{11})|\psi\rangle^{(3)}_{\mathrm{S}} = |\bar{\gamma}_{1111}|^2(\mathcal{N}^2_{2112} + \mathcal{N}^2_{2122})$ is the probability of the event (i.e., PD_{11} clicks). As is clear from Eq. (F6), the state at the input of detector PD_{21} is a vacuum state. Thus, the transmitted information by the first sender (QTx1) is only accessible to the first receiver $j = 1$.

2. Example for Poissonian mixed states: Projective measurement

Consider a Poissonian mixed state as the quantum state of each transmitted signal. Therefore, Eq. (28) for the particular QWDM system presented in Fig. 6 becomes

$$\begin{aligned}
\rho_{\mathrm{C}}^{(3)} &= \prod_{i=1}^{2}\int_0^{2\pi}\frac{d\phi_i}{2\pi}\prod_{j=1,l=1}^{2,2}\hat{D}(\alpha_i\bar{\gamma}_{lsji})|0\rangle^{(3)}\,{}^{(3)}\langle 0|\hat{D}^{\dagger}(\alpha_i\bar{\gamma}_{lsji}) \\
&\approx \int_0^{2\pi}\frac{d\phi_1}{2\pi}\hat{D}(\alpha_1\bar{\gamma}_{1111})\hat{D}(\alpha_1\bar{\gamma}_{1121})|0\rangle^{(3)}\,{}^{(3)}\langle 0| \\
&\quad \times\hat{D}^{\dagger}(\alpha_1\bar{\gamma}_{1111})\hat{D}^{\dagger}(\alpha_1\bar{\gamma}_{1121})\int_0^{2\pi}\frac{d\phi_2}{2\pi}\hat{D}(\alpha_2\bar{\gamma}_{2112}) \\
&\quad \times\hat{D}(\alpha_2\bar{\gamma}_{2122})|0\rangle^{(3)}\,{}^{(3)}\langle 0|\hat{D}^{\dagger}(\alpha_2\bar{\gamma}_{2112})\hat{D}^{\dagger}(\alpha_2\bar{\gamma}_{2122}).
\end{aligned} \tag{F7}$$

Using Eqs. (35) and (E6), the projective measurement $\hat{P}_{11}(\omega_{11})$ on $\rho_C^{(3)}$ leads to

$$\begin{aligned}
&\hat{P}_{11}(\omega_{11})\rho_C^{(3)}\hat{P}_{11}(\omega_{11})\\
&\quad= |1_{11}(\omega_{11})\rangle^{(3)}\,{}^{(3)}\langle 1_{11}(\omega_{11})|\\
&\qquad\times \int \frac{d\phi_1}{2\pi}\frac{d\phi_2}{2\pi} e^{-|c_{111}|^2}|c_{111}\beta_{111}(\omega_{11})|^2\times\cdots\\
&\qquad\times \hat{D}(\alpha_1\bar{\gamma}_{1121})\hat{D}(\alpha_2\bar{\gamma}_{2112})\hat{D}(\alpha_2\bar{\gamma}_{2122})|0\rangle^{(3)}\,{}^{(3)}\langle 0|\\
&\qquad\times \hat{D}^\dagger(\alpha_1\bar{\gamma}_{1121})\hat{D}^\dagger(\alpha_2\bar{\gamma}_{2112})\hat{D}^\dagger(\alpha_2\bar{\gamma}_{2122}).
\end{aligned} \tag{F8}$$

After this projective measurement, the probability that the detector PD_{21} detects one photon with the frequency ω_{11} is not zero since

$$\left|{}^{(3)}\langle 1_{21}(\omega_{11})|\hat{D}(\alpha_1\bar{\gamma}_{1121})|0\rangle^{(3)}\right|^2 = e^{-|\alpha_1\mathcal{N}_{1121}|^2}|\alpha_1\bar{\gamma}_{1121}(\omega_{11})|^2 \neq 0.$$

As a result, the first transmitter (QTx1) can talk simultaneously with both receivers. However, from the security side, the term $\hat{D}(\alpha_1\bar{\gamma}_{1121})|0\rangle^{(3)}\,{}^{(3)}\langle 0|\hat{D}^\dagger(\alpha_1\bar{\gamma}_{1121})$ in Eq. (F8) is related to information leakage in applications such as QKD.

[1] G. Fürnkranz, *The Quantum Internet: Ultrafast and Safe from Hackers* (Springer Nature, Berlin, 2020).
[2] P. P. Rohde, *The Quantum Internet: The Second Quantum Revolution* (Cambridge University Press, Cambridge, UK, 2021).
[3] I. Djordjevic, *Quantum Communication, Quantum Networks, and Quantum Sensing* (Elsevier, Amsterdam, 2022).
[4] M. Razavi, *An Introduction to Quantum Communications Networks*, 2053-2571 (Morgan & Claypool Publishers, California, 2018).
[5] C. A. Brackett, IEEE J. Sel. Areas Commun. **8**, 948 (1990).
[6] M. S. Goodman, H. Kobrinski, M. P. Vecchi, R. M. Bulley, and J. L. Gimlett, IEEE J. Sel. Areas Commun. **8**, 995 (1990).
[7] G. P. Agrawal, *Fiber-Optic Communication Systems*, 5th ed. (John Wiley & Sons, Hoboken, NJ, 2021).
[8] V. Giovannetti, S. Lloyd, L. Maccone, and P. W. Shor, Phys. Rev. A **68**, 062323 (2003).
[9] V. Giovannetti, S. Guha, S. Lloyd, L. Maccone, J. H. Shapiro, and H. P. Yuen, Phys. Rev. Lett. **92**, 027902 (2004).
[10] A. Waseda, M. Takeoka, M. Sasaki, M. Fujiwara, and H. Tanaka, J. Opt. Soc. Am. B **27**, 259 (2010).
[11] X. Wang, IEEE Trans. Inf. Theory **67**, 4524 (2021).
[12] A. Ciurana, J. Martinez-Mateo, M. Peev, A. Poppe, N. Walenta, H. Zbinden, and V. Martín, Opt. Express **22**, 1576 (2014).
[13] R. Asif and W. J. Buchanan, *Recent Progress in the Quantum-to-the-Home Networks* (IntechOpen, London, 2018).
[14] P. D. Townsend, Nature (London) **385**, 47 (1997).
[15] G. Brassard, F. Bussieres, N. Godbout, and S. Lacroix, in *Applications of Photonic Technology 6*, Vol. 5260 (SPIE, Bellingham, WA, 2003), pp. 149–153.
[16] P. L. K. Reddy, B. R. B. Reddy, and S. R. Krishna, Int. J. Comput. Network Inf. Security **4**, 43 (2012).
[17] M. Razavi, IEEE Trans. Commun. **60**, 3071 (2012).
[18] M. Rezai and J. A. Salehi, IEEE Trans. Inf. Theory **67**, 5526 (2021).
[19] B. Fröhlich, J. F. Dynes, M. Lucamarini, A. W. Sharpe, Z. Yuan, and A. J. Shields, Nature (London) **501**, 69 (2013).
[20] N. Hosseinidehaj, Z. Babar, R. Malaney, S. X. Ng, and L. Hanzo, IEEE Commun. Surv. Tutorials **21**, 881 (2018).
[21] M. Alshowkan, B. P. Williams, P. G. Evans, N. S. V. Rao, E. M. Simmerman, H.-H. Lu, N. B. Lingaraju, A. M. Weiner, C. E. Marvinney, Y.-Y. Pai, B. J. Lawrie, N. A. Peters, and J. M. Lukens, PRX Quantum **2**, 040304 (2021).
[22] S. K. Joshi, D. Aktas, S. Wengerowsky, M. Lončarić, S. P. Neumann, B. Liu, T. Scheidl, G. C. Lorenzo, Ž. Samec, L. Kling *et al.*, Sci. Adv. **6**, eaba0959 (2020).
[23] S. Wengerowsky, S. K. Joshi, F. Steinlechner, H. Hübel, and R. Ursin, Nature (London) **564**, 225 (2018).
[24] F. Xu, X. Ma, Q. Zhang, H.-K. Lo, and J.-W. Pan, Rev. Mod. Phys. **92**, 025002 (2020).
[25] Y. Cao, Y. Zhao, Q. Wang, J. Zhang, S. X. Ng, and L. Hanzo, IEEE Commun. Surv. Tutorials **24**, 839 (2022).
[26] B. Qi, W. Zhu, L. Qian, and H.-K. Lo, New J. Phys. **12**, 103042 (2010).
[27] I. Choi, R. J. Young, and P. D. Townsend, Opt. Express **18**, 9600 (2010).
[28] S. Bahrani, M. Razavi, and J. A. Salehi, Sci. Iran. **23**, 2898 (2016).
[29] S. Bahrani, M. Razavi, and J. A. Salehi, Sci. Rep. **8**, 3456 (2018).
[30] G. Cariolaro, *Quantum Communications* (Springer, Berlin, 2015).
[31] W. Kozlowski and S. Wehner, in *Proceedings of the Sixth Annual ACM International Conference on Nanoscale Computing and Communication*, edited by T. M. Christopher Contag (ACM, New York, USA, 2019), pp. 1–7.
[32] F. Centrone, F. Grosshans, and V. Parigi, in *Quantum Information and Measurement VI 2021* (Optica Publishing Group, Washington, DC, 2021), p. W3B.2.
[33] N. B. Lingaraju, H.-H. Lu, S. Seshadri, D. E. Leaird, A. M. Weiner, and J. M. Lukens, Optica **8**, 329 (2021).
[34] J. Capmany, J. Mora, C. R. Fernández-Pousa, and P. Muñoz, Opt. Express **21**, 14841 (2013).
[35] T. Kiss, U. Herzog, and U. Leonhardt, Phys. Rev. A **52**, 2433 (1995).
[36] S. M. Barnett, J. Jeffers, A. Gatti, and R. Loudon, Phys. Rev. A **57**, 2134 (1998).
[37] M. Lasota, R. Filip, and V. C. Usenko, Phys. Rev. A **95**, 062312 (2017).
[38] R. Loudon, *The Quantum Theory of Light* (Oxford University Press, Oxford, UK, 2000).
[39] M. Rezai and J. A. Salehi, IEEE Trans. Quantum Eng. **4**, 1 (2023).
[40] M. de Oliveira, I. Nape, J. Pinnell, N. TabeBordbar, and A. Forbes, Phys. Rev. A **101**, 042303 (2020).
[41] Z.-Y. Zhou, Y. Li, D.-S. Ding, W. Zhang, S. Shi, B.-S. Shi, and G.-C. Guo, Light: Sci. Appl. **5**, e16019 (2016).
[42] R. J. Glauber, Phys. Rev. **131**, 2766 (1963).
[43] G. M. Stéphan, T. T. Tam, S. Blin, P. Besnard, and M. Têtu, Phys. Rev. A **71**, 043809 (2005).

[44] A. Migdall, S. V. Polyakov, J. Fan, and J. C. Bienfang, *Single-Photon Generation and Detection: Physics and Applications* (Academic Press, New York, 2013).
[45] X. Zhang, C. Xu, and Z. Ren, Sci. Rep. **8**, 1 (2018).
[46] C. Chen, E. Y. Zhu, A. Riazi, A. V. Gladyshev, C. Corbari, M. Ibsen, P. G. Kazansky, and L. Qian, Opt. Express **25**, 22667 (2017).
[47] X.-B. Wang, T. Hiroshima, A. Tomita, and M. Hayashi, Phys. Rep. **448**, 1 (2007).
[48] X.-B. Wang, Phys. Rev. Lett. **94**, 230503 (2005).
[49] X. Ma, B. Qi, Y. Zhao, and H.-K. Lo, Phys. Rev. A **72**, 012326 (2005).
[50] W. Liu, J. Peng, P. Huang, D. Huang, and G. Zeng, Opt. Express **25**, 19429 (2017).
[51] N. Peters, P. Toliver, T. Chapuran, R. Runser, S. McNown, C. Peterson, D. Rosenberg, N. Dallmann, R. Hughes, K. McCabe *et al.*, New J. Phys. **11**, 045012 (2009).
[52] K. A. Patel, J. F. Dynes, I. Choi, A. W. Sharpe, A. R. Dixon, Z. L. Yuan, R. V. Penty, and A. J. Shields, Phys. Rev. X **2**, 041010 (2012).
[53] K. Patel, J. Dynes, M. Lucamarini, I. Choi, A. Sharpe, Z. Yuan, R. Penty, and A. Shields, Appl. Phys. Lett. **104**, 051123 (2014).
[54] T. Chapuran, P. Toliver, N. Peters, J. Jackel, M. Goodman, R. Runser, S. McNown, N. Dallmann, R. Hughes, K. McCabe *et al.*, New J. Phys. **11**, 105001 (2009).
[55] J. Malbouisson, S. Duarte, and B. Baseia, Physica A **285**, 397 (2000).
[56] C. Gerry, P. Knight, and P. L. Knight, *Introductory Quantum Optics* (Cambridge University Press, Cambridge, UK, 2005), Chap. 6, p. 138.
[57] T. S. Woodworth, K. W. C. Chan, C. Hermann-Avigliano, and A. M. Marino, Phys. Rev. A **102**, 052603 (2020).
[58] J. Capmany and C. R. Fernández-Pousa, J. Opt. Soc. Am. B **27**, A146 (2010).
[59] A. Jain, P. V. Sakhiya, and R. K. Bahl, in *2020 IEEE International Conference on Electronics, Computing and Communication Technologies (CONECCT)* (IEEE, New York, 2020), pp. 1–5.
[60] M. M. Wilde, *Quantum Information Theory*, 2nd ed. (Cambridge University Press, Cambridge, 2017), pp. xi–xii.
[61] W. H. Zurek, Decoherence and the transition from quantum to classical — revisited, in *Quantum Decoherence: Poincaré Seminar 2005*, edited by B. Duplantier, J.-M. Raimond, and V. Rivasseau (Birkhaüser Basel, Basel, 2007), pp. 1–31.
[62] W. H. Zurek, Entropy **24**, 1520 (2022).
[63] A. K. Ekert, C. M. Alves, D. K. L. Oi, M. Horodecki, P. Horodecki, and L. C. Kwek, Phys. Rev. Lett. **88**, 217901 (2002).
[64] U. Leonhardt, Rep. Prog. Phys. **66**, 1207 (2003).
[65] R. G. Newton, *Scattering Theory of Waves and Particles* (Springer Science & Business Media, Berlin, Heidelberg, 2013), Chap. 2, p. 46.